Modelling polycrystalline solidification using phase field theory

2004 J. Phys.: Condens. Matter 16 R1205

(http://iopscience.iop.org/0953-8984/16/41/R01)

INSTITUTE OF PHYSICS PUBLISHING JOURNAL OF PHYSICS: CONDENSED MATTER

J. Phys.: Condens. Matter **16** (2004) R1205–R1235 PII: S0953-8984(04)73146-X

TOPICAL REVIEW

Modelling polycrystalline solidification using phase field theory

László Gránásy[1], **Tamás Pusztai**[1] **and James A Warren**[2]

[1] Research Institute for Solid State Physics and Optics, PO Box 49, H-1525 Budapest, Hungary
[2] Metallurgy Division, National Institute of Standards and Technology, Gaithersburg, MD 20899, USA

Received 17 March 2004
Published 1 October 2004
Online at stacks.iop.org/JPhysCM/16/R1205
doi:10.1088/0953-8984/16/41/R01

Abstract

We review recent advances made in the phase field modelling of polycrystalline solidification. Areas covered include the development of theory from early approaches that allow for only a few crystal orientations, to the latest models relying on a continuous orientation field and a free energy functional that is invariant to the rotation of the laboratory frame. We discuss a variety of phenomena, including homogeneous nucleation and competitive growth of crystalline particles having different crystal orientations, the kinetics of crystallization, grain boundary dynamics, and the formation of complex polycrystalline growth morphologies including disordered ('dizzy') dendrites, spherulites, fractal-like polycrystalline aggregates, etc. Finally, we extend the approach by incorporating walls, and explore phenomena such as heterogeneous nucleation, particle–front interaction, and solidification in confined geometries (in channels or porous media).

(Some figures in this article are in colour only in the electronic version)

Contents

1. Introduction

Despite thousands of years of experience and more than a hundred years of scientific investigation, the formation of polycrystalline matter (technical alloys, polymers, minerals, etc) is still poorly understood (Cahn 2001). This topical review focuses on recent advances made in modelling polycrystalline solidification. We distinguish here two main types of polycrystalline microstructures.

(a) *Foam-like multigrain structures* formed by impingement of nucleating and growing single crystals. These structures are familiar to all materials scientists, and are a hallmark of equiaxed growth in cast materials.
(b) *Polycrystalline growth forms* in which new grains nucleate at the solidification front.

Examples of such microstructures are shown in figure 1. A typical foam-like structure formed by competing nucleation and growth is displayed in figure 1(a). The polycrystalline dendritic pattern shown in figure 1(b) forms when nucleation is combined with chemical diffusion controlled anisotropic growth. Such a pattern will reduce to something like figure 1(a) if it is allowed to anneal for sufficient time. In contrast, several *polycrystalline growth forms* are presented in figures 1(c)–(j). Particulate additives may transform single-crystal dendrites into polycrystalline *'dizzy' dendrites* (figure 1(c)). *Spherulites* (figure 1(d)), such as those found in such mundane items as plastic grocery bags, provide a classic example of polycrystalline growth. This structure has more generally been observed in a wide variety of materials ranging from pure metals, such as elemental (Se), to nodular cast iron and minerals. The formation of spherulites often starts with the formation of crystal *sheaves* of diverging ends (figure 1(e)), which occasionally develop into less space-filling arboresque structures (figures 1(f) and (g)). Nearly perpendicular random branching, observed in certain polymers, yields 'quadrites' (figure 1(h)). Disorderly growth processes often result in irregular, *fractal-like* structures (figures 1(i) and (j)). The specific mechanisms that lead to the formation of such intricate structures are usually poorly understood. However, nucleation, diffusional instabilities, crystal symmetries, and foreign particles certainly play important roles.

A possible approach to teasing out the dominant controlling influences in the formation of such structures is through mathematical modelling. For this, we need a theoretical framework that is able to incorporate all the important ingredients. Modern theoretical methods combined with the ever-increasing power of computers offer new answers to such problems. Indeed, the phase field theory (PFT) has already demonstrated its ability to describe complex single-crystal morphologies (Boettinger *et al* 2000, 2002, Ode *et al* 2001, Chen 2002). In this topical review, we compile recent results that demonstrate the successful application of this approach to modelling polycrystalline solidification. The paper's structure is detailed below.

First, we briefly introduce the phase field method (section 2.1). This is followed by a review of early models of multi-particle solidification (section 2.2). Subsequently, we outline the use and properties of the orientation field, a generalization to the phase field method that allows for the distinguishing of crystallites with different crystallographic orientations and grain boundary

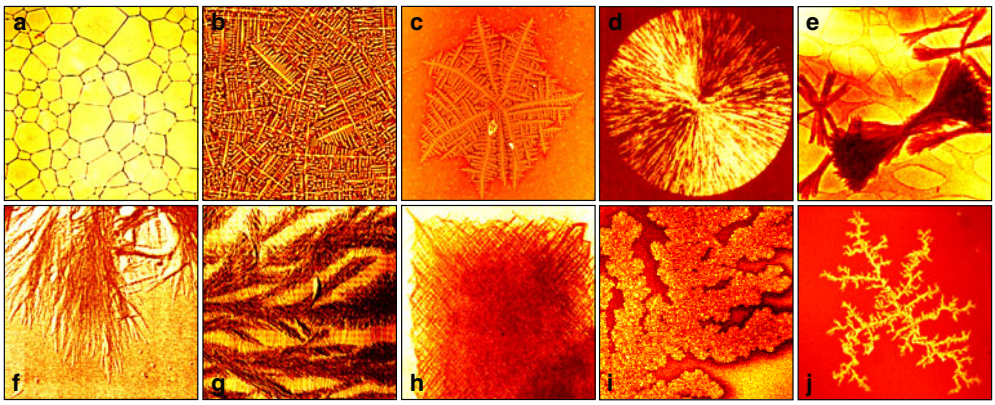

Figure 1. Polycrystalline microstructures. (a) Foam-like morphology formed by competing nucleation and growth (Lee and Losert 2004). (b) Polycrystalline dendritic structure formed by competing nucleation and growth in the oxide glass $(ZnO)_{61.4}\cdot(B_2O_3)_{38.6}\cdot(ZnO_2)_{28}$ (Nobel and James 2003). (c) 'Dizzy' dendrite formed in clay filled polymethyl methacrylate–polyethylene oxide thin film (Ferreiro *et al* 2002). (d) Spherulite formed in pure Se (Ryshchenkow and Faivre 1988). (e) Crystal sheaves in pyromellitic dianhydrite–oxydianilin poly(imid) layer (Ojeda and Martin 1993). (f) Arboresque growth form in polyglycine (Padden and Keith 1965). (g) Polyethylene spherulite crystallized in the presence of n-paraffin (Keith *et al* 1966). (h) 'Quadrite' formed by nearly rectangular branching in isotactic polypropylene (Lotz and Wittmann 1986). (i) Fractal-like polycrystalline aggregate of electrodeposited Cu (Fleury 1997). (j) Polycrystalline fractal-like growth form observed in clay filled polyethylene oxide–polymethyl methacrylate film (Ferreiro *et al* 2002). To improve the contrast/visibility of the experimental pictures, they are shown here in false colour.

properties (section 2.3). In section 2.4, we address possible approaches to homogeneous crystal nucleation, including a quantitative test of theory based on a comparison with atomistic simulations. Results concerning the competitive growth of continuously nucleating particles (formation of foam-like structures) as well as the kinetics of crystallization are reviewed in section 2.5. The formation of polycrystalline growth morphologies (sheaves, axialites, fractal-like aggregates, spherulites, etc) characteristic to far-from-equilibrium solidification and the essential factors that govern polycrystalline solidification are covered in section 2.6. Grain boundary dynamics and heterogeneous nucleation on walls/foreign particles are addressed in sections 2.7 and 2.8, respectively. Finally, promising ideas that may set future trends of theoretical development are highlighted in section 3.

2. Phase field theory of polycrystalline solidification

2.1. Field theoretic approach to crystal growth

The phase field technique is described in a number of recent reviews (Boettinger *et al* 2000, 2002, Ode *et al* 2001, Chen 2002, Emmerich 2003). Here we recall only its main features needed for understanding later developments. The phase field theory is a direct descendant of the Cahn–Hilliard/Ginzburg–Landau type classical field theoretic approaches to phase boundaries, and its origin can be traced back to a model of Langer from 1978 (see Langer 1986) and others (Collins and Levine 1985, Caginalp 1986). To characterize the local phase state of matter, a non-conserved structural order parameter $\phi(\mathbf{r}, t)$ termed the phase field is introduced. This structural order parameter is considered to be a measure of local crystallinity, and is often interpreted as the volume fraction of the given crystalline phase. While much

depends on the approach, a minimum of n structural fields are needed $\{\phi_i(\mathbf{r}, t)\}$ in the presence of n crystalline phases, and one disordered phase. Certain approaches, such as the multi-phase field theory by Steinbach *et al* (1996), introduce a separate phase field for every crystal grain, and can require thousands of phase fields to properly address multi-grain problems. Even then, such multi-phase field theories cannot naturally accommodate the formation of new, randomly oriented grains.

One expands the free energy density (or entropy density) of the inhomogeneous system (liquid + solid phase(s)) with respect to the structural order parameter(s) $\{\phi_i\}$, the chemical composition field(s) $\{c_i\}$, the orientation field, etc, retaining only those spatial derivatives that are allowed by symmetry considerations. The free energy of the system is thus a local functional of these fields:

$$F = \int \mathrm{d}\mathbf{r} \left\{ \sum_{i,j} a_{ij}(\nabla\phi_i \nabla\phi_j) + \sum_{i,j} b_{ij}(\nabla c_i \nabla c_j) + \cdots + f[\{\phi_i\}, \{c_i\}, T, \ldots] \right\}. \tag{1}$$

The terms that contain the field gradients account for the interfacial energies. The coefficients a_{ij} and b_{ij} may depend on temperature, orientation, and the field variables. The free energy density $f(\{\phi_i\}, \{c_i\}, T, \ldots)$ shows two or more minima that represent bulk liquid and crystalline phases. While attempts have been made to derive the free energy functional of solid–liquid systems on physical grounds (density functional theory; review: Oxtoby 1991, 2002), the molecular theories are often too complicated to address complex solidification problems. Therefore, in most approaches a phenomenological free energy (or entropy) functional is used, whose form owes much to the Ginzburg–Landau models used in describing magnetic phase transitions and phase separation (Gunton *et al* 1983). Each phase field approach usually differs in both the field variables considered as well as the actual form chosen for their interaction. Once the free energy functional is defined, the formalism that describes the time evolution follows almost automatically.

Following the phenomenology of non-equilibrium statistical mechanics, and relying on the principle of positive entropy production (or decreasing free energy), partial differential equations are derived for the evolution of the phase field and other field variables like concentration or temperature (Langer 1986, Penrose and Fife 1990, Kobayashi 1993, Wang *et al* 1993, Elder *et al* 1994, Warren and Boettinger 1995, Caginalp and Jones 1995). The equation of motion differs for non-conserved fields (such as the structural order parameter, orientation, magnetization, etc whose spatial integral may vary with time) and conserved fields (whose spatial integral is constant, e.g., chemical composition):

$$\text{Non-conserved dynamics: } \dot{\phi}_i = -M_{\phi_i} \frac{\delta F}{\delta \phi_i} + \zeta_i$$

$$\text{Conserved dynamics: } \dot{c}_i = \nabla \left\{ M_{c_i} \nabla \frac{\delta F}{\delta c_i} \right\} + \zeta_{j_c}.$$

Here M_i are the appropriate field mobilities, and we have made the simplifying assumption that there are no mobility cross couplings between the $\phi_{i,}$ or between the c_i. The ζ_i are Gaussian noise terms (random current for conserved quantities) with an amplitude determined by the fluctuation–dissipation theorem. (On the latter see Elder *et al* 1994, Karma and Rappel 1999, Pavlik and Sekerka 1999, 2000; on the Langevin formalism in general van Kampen 2003.) The evolution of the non-conserved phase variables ϕ_i is thus coupled to those of the conserved fields (generalized Hohenberg–Halperin model C-type field theory; Hohenberg and Halperin 1977). These equations of motion are usually highly non-linear, and are able to describe complex solidification morphologies such as thermally controlled dendrites (Kobayashi 1993, 1994, Karma and Rappel 1998, Bragard *et al* 2002) and solutal dendrites (Warren and Boettinger

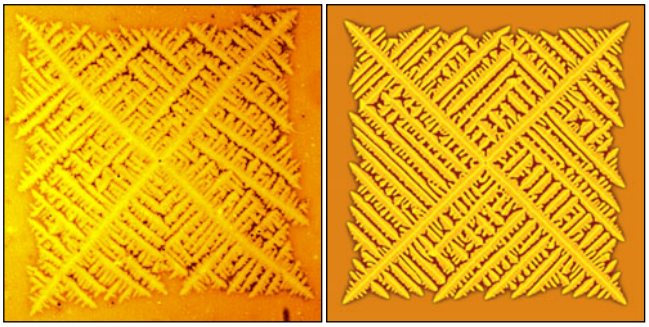

Figure 2. Single-crystal dendrites in polymethyl methacrylate–polyethylene oxide film (Ferreiro *et al* 2002) and in a phase field simulation performed on a 2000 × 2000 rectangular grid (26.3 μm × 26.3 μm) at 1574 K and supersaturation $S = (c_l - c_\infty)/(c_l - c_s) = 0.80$ using the thermodynamic and interfacial properties of Ni–Cu, and a 15% anisotropy for the interfacial free energy. Here c_∞, c_l, and c_s are the initial composition of the liquid, and the liquidus and solidus compositions. (For details see Gránásy *et al* (2003c).) The simulation has been made using model B (see the appendix).

1995, Conti 1997, Loginova *et al* 2001, Suzuki *et al* 2002) (see figure 2), eutectic growth patterns (Karma 1994, Elder *et al* 1994, Wheeler *et al* 1996, Drolet *et al* 2000, Apel *et al* 2002, Plapp and Karma 2002) and peritectic growth patterns (Nestler and Wheeler 2000, Lo *et al* 2001, 2003), banded structures (Conti 1998), and many more. However, one of the main challenges to the successful application of the phase field method to microstructure formation is the quantitative prediction of these processes, which has a vast practical importance in optimizing and designing materials for specific applications.

The primary barrier to accurate, quantitative phase field modelling is resolving the interface thickness. The diffuseness of the interface is an essential feature of phase field models, and is due to the square-gradient terms, which penalize sharp changes in the fields. Experiments (Howe 1996, Huisman *et al* 1997) and computer simulations (Broughton *et al* 1982, Laird and Haymet 1992, Davidchack and Laird 1998) show that the crystal/liquid interface is indeed diffuse on the molecular scale; the interface region extends to a few nanometres. This is, however, usually orders of magnitude smaller than the objects of interest; therefore, practically, a sharp interface is usually an excellent approximation. Thus numerical solution of the equations, at the resolution required to describe the nanometre thick diffuse interfaces properly, is, as yet, impossible (in two and higher dimensions) even with the most powerful computers. Thus, an artificially broad interface has to be used, i.e., the interface thickness is usually regarded as a model parameter. Therefore, care must be taken to ensure that the diffuse interface calculations deliver the proper interface dynamics. Methods have been worked out to ensure this by adjusting the model parameters and introducing interface currents (i.e., a new term in the phase field equations) to compensate for the unphysical effects of a too thick interface (Karma and Rappel 1996, 1998, Karma 2001). Such techniques allow for a *quantitative* modelling of dendrites and eutectic solidification in the framework of the phase field theory (Karma and Rappel 1998, Bragard *et al* 2002, Folch and Plapp 2003). Another important challenge to quantitative phase field modelling is associated with the application of theory under strong anisotropies of the interface free energy and/or kinetic coefficient and the related phenomenon of faceting (Kobayashi and Giga 2001, Eggleston *et al* 2001, Uehara and Sekerka 2003, Debierre *et al* 2003).

It is worth noting that although the phase field theory is a phenomenological model, it can be derived on physical grounds using a density functional approach. Viewing the crystal

as a highly inhomogeneous liquid, with peaks at the lattice sites, the Fourier amplitudes of the number density appear as natural order parameters. Their number can be reduced if one assumes that the density peaks at the atomic sites have a Gaussian form. In this case, all Fourier amplitudes of the number density can be expressed uniquely in terms of the amplitude of the dominant density wave, thus a single structural order parameter suffices (Khachaturyan 1996, Shen and Oxtoby 1996). Thus, the phase field can be viewed as the amplitude of the dominant Fourier component of the singlet density in the crystal. A possible route to obtain the free energy functional on physical grounds is outlined by Shih *et al* (1987) on the basis of a Ginzburg–Landau expansion that considers crystal symmetries. This also offers physical interpretation for the model parameters, and derivation of the functions introduced intuitively. Formulation of a single order parameter theory of bcc and fcc nucleation along this line has been presented recently (Gránásy and Pusztai 2002). Various aspects of linking atomistic simulations with field theory are addressed by Hoyt and Asta (2002) and Hoyt *et al* (2003).

With the possible exception of the multi-phase field theory, none of the models mentioned above are able to describe anisotropic growth of crystal grains with different crystallographic orientations. Due to the practical importance of polycrystalline materials, extensive efforts have been made to extend the phase field approach to this case.

2.2. Early models of polycrystalline solidification

Polycrystalline solidification can be addressed at different levels, as is implied by the varying complexity of the polycrystalline morphologies shown in figure 1.

Foam-like multigrain structures emerge in the presence of competing nucleation and growth. Such problems are traditionally addressed in the framework of Johnson–Mehl–Avrami–Kolmogorov (JMAK) theory (for review see Christian 1981). The 'overlapping' crystalline fraction is given by the integral

$$Y(t) = \frac{4\pi}{3} \int_0^t J(\tau) \left\{ R^* + \int_\tau^t v(\vartheta)\, \mathrm{d}\vartheta \right\}^3 \mathrm{d}\tau, \tag{2}$$

where J, v, and R^* are the nucleation rate and growth rate, and the radius of the critical fluctuation, while the integration variables ϑ and τ have dimensions of time. This expression coincides with the true crystalline fraction X at the beginning of the process, when the crystalline particles grow independently. However, soon the regions overlap, and multiply covered volumes form, and equation (2) overestimates the true crystalline fraction. A simple mean field correction relating X and Y through the expression $\mathrm{d}X = (1 - X)\,\mathrm{d}Y$ counts only that fraction of $\mathrm{d}Y$ that falls on the untransformed region. This immediately yields $X = 1 - \exp\{-Y\}$. This mean field approach is exact if (i) the system is infinite; (ii) the nucleation rate is spatially homogeneous; and (iii) either a common time dependent growth rate applies or anisotropically growing convex particles are aligned in parallel (for derivation with the time cone method, see Cahn 1996, 1997). Then, for constant nucleation and growth rates in infinite systems, the time evolution follows the JMAK scaling $X = 1 - \exp\{-(t/t_0)^p\}$, where t_0 is a time constant, $p = 1 + d$ is the Kolmogorov exponent, and d is the number of dimensions, while, for the problem of a fixed number of nuclei, the same expression applies with $p = d$. One of the interesting questions is to what degree JMAK scaling applies in the presence of chemical diffusion. Condition (iii) is obviously violated here, as diffusion-controlled growth yields a growth rate that depends on particle size. While no exact treatment is available, it has been suggested (Christian 1981) that under such conditions, $p \approx 1 + d/2$ applies for constant nucleation rate and $p \approx d/2$ for fixed number of particles. Recent experimental studies find, however, deviation from this behaviour for diffusion mediated 'soft

Figure 3. Various views (left and centre) and a contour line map (right) of the free energy landscape of the 'jello-mould' type model by Morin *et al* (1995). The central minimum represents the liquid, while the other minima correspond to different crystallographic orientations. (The phase field is the radial distance from the centre, and the angle is the orientational variable.)

impingement' of crystal particles (Pradell *et al* 1998). It is straightforward to use the phase field theory to explore such problems.

PFTs with isotropic growth. (In this limiting case one does not need the local crystallographic orientation to develop the model.) Jou and Lusk (1997) studied the formation of foam-like multigrain structures in a one-component, isotropic system using a scalar order parameter theory. They found minor deviations at small times from a constant growth rate, and also found that the transformed fraction essentially follows the JMAK scaling, except in the case of large nucleation rates. Elder *et al* (1994) modelled multigrain solidification in an isotropic eutectic system using a structural order parameter, a concentration field, and Langevin noise induced crystal nucleation. The Kolmogorov exponent $p = 3$ they find is consistent with the absence of long-range diffusion. (Only short-range diffusion, parallel with the growth front, plays a role here.) Gránásy *et al* (2001) studied competing growth of fixed number of particles in an isotropic binary system. A free energy based phase field theory, equivalent with the entropy formulation of Warren and Boettinger (1995), has been used. They reported that the Kolmogorov exponent decreases with increasing transformed fraction, a behaviour that resembles the trends seen in experiment (Pradell *et al* 1998).

PFTs with anisotropic growth. In order to handle nucleation and growth of more than one anisotropically growing particle (see figure 1(b)), crystallographic orientations need to be included in the theory.

The first phase field model that allowed for different crystallographic orientations in a solidifying system is due to Morin *et al* (1995). In this treatment, the free energy density has n wells, corresponding to n crystallographic orientation that breaks the rotational symmetry of the free energy (figure 3). Seeds of fixed critical size were randomly introduced in space and time to mimic homogeneous nucleation. The model has been applied for polymorphous crystallization, where the composition of the liquid is close to that of the crystal. Accordingly, chemical diffusion plays a minor role and the JMAK form fits to the simulations with a Kolmogorov exponent corresponding to homogeneous nucleation. A drawback of the model is that the rotational symmetry of the free energy had to be sacrificed to obtain a finite number of crystallographic orientations, with a diffuse interface between grains.

The multi-phase field models (Steinbach *et al* 1996, Fan and Chen 1996, Krill and Chen 2002) are extremely flexible approaches that can be used to describe nucleation and growth of particles with random crystallographic orientation. To our knowledge, these models have not been applied for such problems. They have, however, been successfully used to describe the time evolution of multigrain structures (grain boundary dynamics). Difficulties arise, however,

due to the large number of phase fields if one intends to use Langevin noise to initiate nucleation. Although this can certainly be substituted by inserting the nuclei by 'hand', this becomes rather tedious when structures that require the nucleation of different crystallographic orientations at the growth front (figures 1(c)–(j)) are to be addressed. This model also effectively breaks the rotational symmetry of the free energy, for a given number of phase fields.

Below we describe further advances in the theory of polycrystals, particularly in the directions of restoring the rotational invariance of the free energy and incorporating a natural (noise driven) nucleation of new crystal orientations.

2.3. Orientation field and the associated free energy

The first model of polycrystalline solidification that both incorporates crystallographic orientation and has a rotationally invariant free energy is due to Kobayashi *et al* (1998). Since this is the basis for further developments, it is discussed here in detail.

To handle crystallographic orientation in two dimensions, a non-conserved orientation field $\theta(\mathbf{r}, t)$ is introduced whose local value specifies the orientation angle that, in turn, sets the tilt of the crystal planes in the laboratory frame. Accordingly, the angular dependence of the interfacial free energy and/or the kinetic coefficient needed for addressing anisotropic growth is measured relative to this orientation. The orientational free energy F_{ori} is now derived using a heuristic approach. Following the philosophy of the phase field method, we require that the free energy is a local functional, i.e., it may depend on only the field variables and their derivatives, while non-local interactions that would yield integro-differential equation of motion are not considered. Since we wish to retain the invariance of free energy to rotation, we have to exclude an explicit dependence on θ and its powers. We seek the orientational free energies in the form $F_{\text{ori}} = \int \mathrm{d}\mathbf{r}\, H|\nabla\theta|^n$, where H and n are not yet specified. Considering a planar interface between two semi-infinite crystal grains (a bicrystal) of misorientation $\Delta\theta$, one finds that

$$F_{\text{ori}} = \int_0^L \mathrm{d}x\, H|\nabla\theta|^n \propto \frac{(\Delta\theta)^n}{L^{n-1}}, \tag{3}$$

where spatial integration is taken along the spatial coordinate x perpendicular to the interface, while the thickness of the interface region is L. Thus, for $n > 1$, the orientation free energy diminishes with increasing interface thickness, i.e., the system tends to lower its free energy by broadening the interface indefinitely. It should be noted that $n = 2$ is actually a fine model for a grain boundary, with the caveat that real grain boundaries are properly described as a wall of dislocations. Dislocations are singularities in the $\nabla\theta$ field, and we do not wish to model each dislocation in our system, only coherent lines of dislocations (grain boundaries). Thus, the most plausible choice that leads to a stable interface with non-zero free energy is $n = 1$. In this case, the orientational free energy of the interface is proportional to $\Delta\theta$ (see figure 4(a)), provided that $\theta(x)$ is monotonic (if $\theta(x)$ is non-monotonic, the energy is not a minimum). This leaves, however, the interface profile $\theta(x)$ still arbitrary. This arbitrariness can be remedied if we assume that the coefficient H has a minimum at the position of the interface (see figure 4(b)). Then, the minimization of free energy will lead to a stepwise variation of $\theta(x)$, a behaviour approximating reasonably the experimental reality of stable, flat grain boundaries. Such a minimum can be realized either making the coefficient H dependent on the solid–liquid structural order parameter, or on an extra field that determines whether the solid material is crystalline or disordered (Kobayashi *et al* 1998). However, due to the non-analytic nature of this orientational free energy density, the equation of motion specifies a *singular diffusivity* problem, and requires special care when handled numerically (Kobayashi and Giga 1999). Various modifications of this approach have been applied to describe competing growth

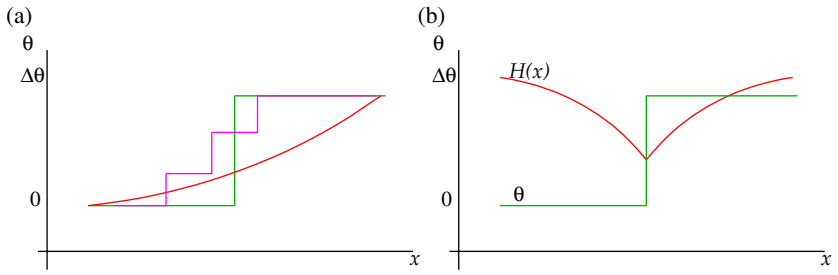

Figure 4. (a) $\int dx\,|\nabla\theta| = |\Delta\theta|$ is the same for the three $\theta(x)$ functions (single-step, multi-step, curved), since they vary monotonically between the same end points. (b) If the coefficient of $|\nabla\theta|$ has a minimum in the interface—after free energy minimization—the orientation field changes stepwise between the two orientations.

of anisotropic particles, including dendritic solidification in undercooled single-component (Kobayashi *et al* 1998) and binary liquids (Warren *et al* 2003b). Applications to grain boundary problems including grain boundary wetting and grain coarsening in polycrystalline matter via grain boundary migration and rotation are reviewed in section 2.7 (Warren *et al* 2003a). The model used for the latter studies will be called model A, and is described in the appendix. *Note that the models termed models A to C in this paper differ from models A to C of the usual* Hohenberg and Halperin (1977) *classification of classical field theories.*

The modelling of nucleation of grains at the solidification front requires a further important ingredient. This ingredient was introduced by Gránásy *et al* (2002a, 2002b), who extended the orientation field θ into the liquid phase, where it fluctuates in time and space. Assigning local crystal orientation to liquid regions, even a fluctuating one, may seem artificial at first sight. However, due to geometrical and/or chemical constraints a short-range order exists even in simple liquids, which is often similar to the one in the solid. Rotating the crystalline first-neighbour shell so that it aligns optimally with the local liquid structure, one may assign a local orientation to every atom in the liquid. The orientation obtained in this manner fluctuates in time and space. The correlation of the atomic positions/angles shows how good this fit is. (In the model, the fluctuating orientation field and the phase field play these roles.) Approaching the solid from the liquid, the orientation becomes more definite (the amplitude of the orientational fluctuations decreases) and matches to that of the solid, while the correlation between the local liquid structure and the crystal structure improves. In this model, called model B henceforth (for details see the appendix), the orientation field and the phase field are strongly coupled to recover this behaviour.

In model B, the free energy density was assumed to have the form $f_{\rm ori} = HT[1 - p(\phi)]|\nabla\theta|$, where $p(\phi)$ is the phase interpolation function (see the appendix) that varies between zero and unity, while ϕ changes from zero to unity corresponding to the bulk solid and liquid states, respectively. The free energy of the small angle grain boundaries scales with HT. Note that due to the $[1 - p(\phi)]$ multiplier, the driving force of orientational ordering disappears in the liquid. This is needed to avoid double counting of the orientational contribution in the liquid, which is *per definitionem* taken into account in the free energy difference between the bulk liquid and solid phases. Since we are primarily interested in polycrystalline solidification that takes place on a far shorter timescale than grain boundary relaxation, the orientational mobility is assumed to vary proportionally to $p(\phi)$ across the interface (set zero in solid and maximum in liquid). Accordingly, orientational ordering takes place exclusively at the crystal–liquid interface, concurrently with structural ordering. An important consequence is that, in general, there is a contribution to the free energy of the solid–liquid interface emerging from the

orientational noise in the interface region. With appropriate choice of the model parameters, however, an orientationally ordered liquid layer develops ahead of the solidification front (as observed in molecular dynamics simulations, see e.g. Laird and Haymet 1992, Davidchack and Laird 1998), rendering this contribution insignificant. Then the usual simple relationships between interfacial properties (thickness and free energy) and the model parameters can be retained.

The introduction of the orientational field and the respective mobility are accompanied with the appearance of *additional time* and *length scales*. The relaxation time of orientational perturbations is inversely proportional to the orientational mobility M_θ, which in turn is proportional to the *rotational* diffusion coefficient $M_\theta \propto D_{\mathrm{rot}}$ of molecules. It appears that this new timescale plays an essential role in the formation of many polycrystalline structures. Recently, it has become appreciated that undercooled liquids of sufficiently high viscosity ($\approx$30–50 Pa s) exhibit spontaneous and long-lived heterogeneities, associated with the formation of regions within the fluid having much higher and lower mobility relative to a simple fluid in which particles exhibit Brownian motion (Donati *et al* 1998, Bennemann *et al* 1999). These *dynamic heterogeneities* persist on timescales of the order of the stress relaxation time, which can be minutes near the glass transition and astronomical times at lower temperatures. The presence of such transient heterogeneities has been associated with dramatic changes in the transport properties of supercooled liquids (Rössler 1990, Chang and Sillescu 1997, Masuhr *et al* 1999, Ngai *et al* 2000, Swallen *et al* 2003). Specifically, both the translational diffusion coefficient D_{tr} and the rotational diffusion coefficient D_{rot} (quantities associated with the rate of molecular translation and rotation in the liquid) scale with the inverse of liquid shear viscosity (Stokes–Einstein and Stokes–Einstein–Debye relation-ships) at high T and low undercooling, but D_{rot} slows down significantly relative to D_{tr} at lower T. This phenomenon in cooled liquids is termed 'decoupling' (Rössler 1990, Chang and Sillescu 1997, Masuhr *et al* 1999, Ngai *et al* 2000, Swallen *et al* 2003). As a result, at low temperatures, where rotational relaxation is slow relative to the translational one that governs the growth rate, orientational defects (e.g. new grains) can be frozen into the solid. Model B naturally incorporates this possibility (the orientational mobility needs to be reduced relative to the phase field mobility). As will be demonstrated in section 2.6, model B is able to recover many of the polycrystalline morphologies via this mechanism. Before this, however, we explore the applicability of the phase field formalism to nanometre size fluctuations that govern crystal nucleation.

2.4. Homogeneous crystal nucleation

The crystallization of a homogeneous undercooled liquid starts with the formation of *heterophase fluctuations* whose central part evinces crystal-like atomic arrangement. Those fluctuations that exceed a critical size, determined by the interplay of the interfacial and volumetric contributions to the cluster free energy, have a good chance of reaching macroscopic dimensions, while the smaller clusters decay with a high probability. Critical size heterophase fluctuations are termed *nuclei* and the process in which they form via internal fluctuations of the liquid is *homogeneous nucleation* (as opposed to the *heterogeneous nucleation*, where particles, foreign surfaces, or impurities help to produce the heterophase fluctuations that drive the system towards solidification). The description of the near-critical fluctuations is problematic even in one-component systems. The main difficulty is that critical fluctuations forming on reasonable experimental timescales contain typically a few times ten to several hundred molecules (Báez and Clancy 1995, ten Wolde *et al* 1995, 1996, Auer and Frenkel 2001a, 2001b). This together with the fact that the crystal–liquid interface extends to several molecular layers (Laird and Haymet 1992, Davidchack and Laird 1998) indicates that the

critical fluctuations are essentially comprised of interface. Therefore, the droplet model of classical nucleation theory, which employs a sharp interface separating a liquid from a crystal with bulk properties, is certainly inappropriate for such fluctuations as demonstrated by recent atomistic simulations (Auer and Frenkel 2001a, 2001b). Field theoretic models that predict a diffuse interface offer a natural way to handle such difficulties (Oxtoby 2002). Here, we review recent applications of the phase field theory for describing homogeneous crystal nucleation, and address two possibilities.

(a) The phase-field theory can be used to *simulate* the nucleation process. The proper statistical mechanical treatment of the nucleation process requires the introduction of uncorrelated Langevin-noise terms into the governing equations with amplitudes that are determined by the fluctuation–dissipation theorem (Elder *et al* 1994, Drolet *et al* 2000, Pavlik and Sekerka 1999, 2000). Such an approach has been used for describing homogeneous nucleation in a single-component system (Castro 2003) and during eutectic solidification in a binary model (Elder *et al* 1994, Drolet *et al* 2000). However, modelling of nucleation via Langevin noise is often prohibitively time consuming. One remedy is simply to increase the amplitude of the noise. This, however, raises the possibility that the fluctuations, which initiate solidification, will most likely significantly differ from the real critical fluctuations. To avoid practical difficulties associated with modelling noise-induced nucleation, crystallization in simulations is often initiated by randomly placing supercritical particles into the simulation window (e.g. Simmons *et al* 2000, Lo *et al* 2001, 2003). An alternative method has been proposed by Gránásy *et al* (2002a, 2002b), who first calculate the properties of the critical fluctuations (see below) and then place such critical fluctuations randomly into the simulation window, while also adding Langevin noise that decides whether these nuclei grow or dissolve.

(b) Besides *simulating* the nucleation process, the phase field theory can be used to *calculate the height of the nucleation barrier* (Roy *et al* 1998, Gránásy *et al* 2002a, 2002b, 2003b). Being in unstable equilibrium, the critical fluctuation (the nucleus) can be found as an extremum of the free energy functional, subject to conservation constraints when the phase field is coupled to conserved fields. To mathematically impose such constraints one adds the volume integral over the conserved field times a Lagrange multiplier to the free energy. The field distributions, that extremize the free energy, obey the appropriate Euler–Lagrange equations, which in the case of local functionals, used in the phase field theory, take the form

$$\frac{\delta F}{\delta \chi} = \frac{\partial \omega}{\partial \chi} - \nabla \frac{\partial \omega}{\partial \nabla \chi} = 0, \tag{4}$$

where $\delta F/\delta \chi$ stands for the first functional derivative of the free energy with respect to the field χ, while ω is the total free energy density (incorporating the gradient terms). Here χ stands for all the fields used in theory. The Euler–Lagrange equations are solved assuming that unperturbed liquid exists in the far field, while, for symmetry reasons, zero field gradients exist at the centre of the fluctuations. The same solutions can also be obtained as the non-trivial time-independent solution of the governing equations for field evolution. Having determined the solutions, the work of formation of the nucleus (height of the nucleation barrier) can be obtained by inserting the solution into the free energy functional.

While in large-scale simulations one is often compelled to use an unphysically broad interface, in the case of nucleation, where the interface thickness and the size of nuclei are comparable, one can work with the physical interface thickness. In a few cases, all parameters

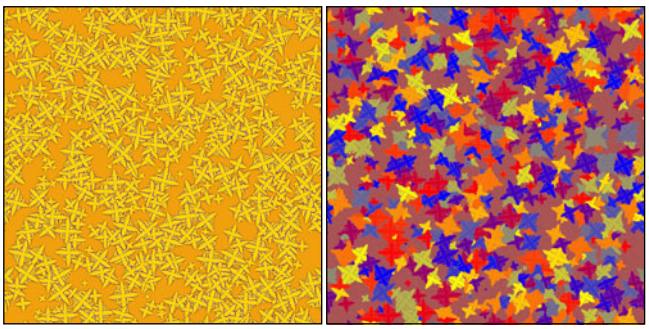

Figure 5. Snapshots of the concentration (left) and orientation (right) fields for two-dimensional dendritic solidification of a binary alloy (Ni–Cu) as predicted by model B at 1574 K and supersaturation 0.78. By the end of solidification ∼700 dendritic particles formed. The calculation has been performed on a 7000 × 7000 grid (92.1 μm × 92.1 μm) with a 5% anisotropy of the interfacial free energy that was assumed to have a fourfold symmetry. (Colouring: on the left, yellow and blue correspond to the solidus and liquidus compositions, respectively, while the intermediate compositions are shows by colours that interpolate linearly between these colours. On the right, colours denote crystallographic orientations: When the fast growth direction is upward, 30°, or 60° left, the grains are coloured blue, yellow, or red, respectively, while the intermediate angles are denoted by a continuous transition among these colours. Owing to the fourfold symmetry, orientations that differ by 90° multiples are equivalent.)

of the phase field theory can be fixed, and the calculations can be performed without adjustable parameters. For example, in the one-component limit of the standard binary phase field theory (Warren and Boettinger 1995), the free energy functional contains only two parameters, the coefficient of the square-gradient term for phase field and the free energy scale (height of the central hill between the double well in the local free energy density). If the thickness and the free energy of a crystal–liquid interface are known for the equilibrium crystal–liquid interface, all model parameters can be fixed and the properties of the critical fluctuation, including the height of the nucleation barrier, can be predicted without adjustable parameters. Such information is available from atomistic simulations/experiments for a few cases (Lennard-Jones system and ice–water system). This procedure leads to a good quantitative agreement with the magnitude of the nucleation barriers deduced from atomistic simulations for the Lennard-Jones system, and from experiments on ice nucleation in undercooled water (Gránásy *et al* 2002a). A similar approach for a binary Ni–Cu alloy led to reasonable values for the temperature and composition dependence of the interface free energy of critical fluctuations, and also yielded reasonable critical undercoolings for electromagnetically levitated droplets (Gránásy *et al* 2002a). Similar results have been obtained for the hard-sphere system using a phase field model that relies on a structural order parameter coupled to the density field (Gránásy *et al* 2003b).

These findings suggest that, using the physical interface thickness, the phase field theory is able to predict the height of the nucleation barrier quantitatively.

2.5. Competing nucleation and growth

The kinetics of anisotropic solidification in a binary system has been studied in two dimensions by Gránásy *et al* (2002a, 2002b, 2003a) using model B. A typical polycrystalline dendritic morphology closely resembling figure 1(b) is shown in figure 5. The large number of particles (∼700) provides reasonable statistics to evaluate the Kolmogorov exponent p. Four representative simulations performed on a 7000 × 7000 grid are compared (Gránásy *et al* 2003a): two simulations were performed for a reduced concentration of

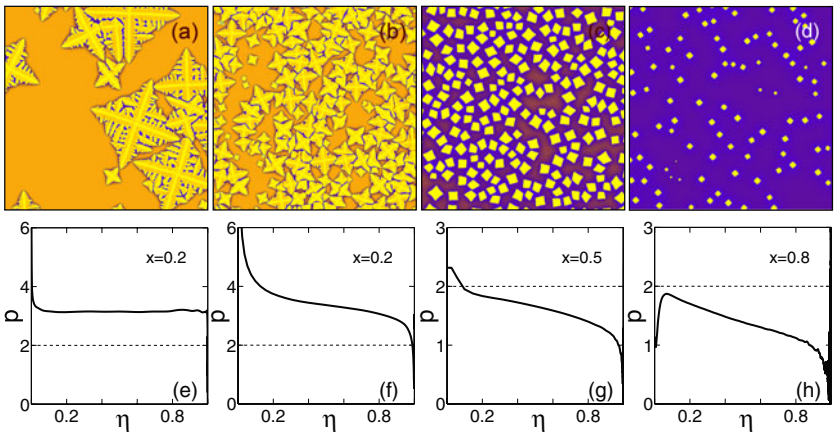

Figure 6. Two-dimensional anisotropic multigrain solidification as a function of composition and nucleation rate in the Cu–Ni system at 1574 K as predicted by model B. (a)–(d) 1000 × 1000 segments (13.2 μm × 13.2 μm) of the concentration distribution (yellow—solidus; blue—liquidus) and (e)–(h) the respective Kolmogorov exponent versus normalized transformed fraction curves are shown. Simulations presented in panels (a) and (b) differ in the magnitude of the nucleation rate.

$x = (c_\infty - c_s)/(c_l - c_s) = 0.2$ between the solidus and liquidus (c_∞ is the composition of the initial liquid, $c_s = 0.399\,112$ and $c_l = 0.466\,219$ are the solidus and liquidus compositions at $T = 1574$ K), while the others at 0.5 and 0.8. 1000×1000 sections of the respective simulations are shown in figure 6 (panels (a)–(d)), together with the respective Komogorov exponents evaluated as a function of the normalized crystalline fraction $\eta = X/X_{max}$, (panels (e)–(h)), where X_{max} is the maximum crystalline fraction achieved at the given liquid composition.

If the nucleation rate is low enough there is space to develop a full dendritic morphology (figure 6(a)). Note that in the case of dendritic solidification, the global average of the composition of the growing solid combined with the interdendritic liquid trapped between the dendrite arms must be equal to the initial composition of the liquid, thus solute pile up does not decelerate the advance of the perimeter (except as a transient). Since the dendrite tip is a steady state solution of the diffusion equation, constant nucleation and growth rates apply, and thus $p = 1+d = 3$ is expected in two dimensions. Indeed, the observed Kolmogorov exponent is $p \approx 3$. In the other simulations, the particles have a more compact shape, and interact via their diffusion fields, a phenomenon termed 'soft impingement'. The respective Kolmogorov exponents decrease with increasing solid fraction. A closer inspection of the process indicates that at large supersaturations where there is no substantial difference in the composition of the nucleus and the initial liquid (see figures 6(b) and (f)), growth in the initial stage right after nucleation, is interface controlled (governed by the phase field mobility), as opposed to control by chemical diffusion. This results in a delay in the onset of diffusion-controlled growth, resulting in a value for p that decreases with time; a phenomenon that becomes weaker with decreasing supersaturation. This effect will only be perceptible in the case of copious nucleation, where the length of this transient period is comparable to the total solidification time. Indeed, such behaviour has been observed during the formation of nanocrystalline materials made by the devitrification of metallic glass ribbons (Pradell *et al* 1998).

2.6. Polycrystalline growth morphologies

Particulate additives can be used to initiate nucleation and they find application as grain refiners for many practical systems. Recent experiments on clay filled polymer blend films revealed

that, besides this role, they may also perturb crystal growth, yielding polycrystalline growth morphologies (Ferreiro *et al* 2002). Polycrystalline growth also occurs in pure liquids in the absence of particulate additives (e.g. Keith and Padden 1963, Ryshchenkow and Faivre 1988, Magill 2001). Both routes to *polycrystalline growth* have recently been addressed within the framework of the phase field theory.

2.6.1. Effect of foreign particles. A spectacular class of structures appears in thin polymer blend films, if foreign (clay) particles are introduced. This disordered dendritic structure is termed a 'dizzy' dendrite (figure 1(c)). These structures are formed by the engulfment of the clay particles into the crystal, inducing the formation of new grains. This phenomenon is driven by the impetus to reduce the crystallographic misfit along the perimeter of clay particles by creating grain boundaries within the polymer crystal. This process changes the crystal orientation at the dendrite tip, changing thus the tip trajectory ('tip deflection'). To describe this phenomenon, Gránásy *et al* (2003c) incorporated a simple model of foreign crystalline particles into model B: they are represented by *orientation pinning centres*—small areas of random, but fixed orientation—which are assumed to be of a foreign material, and not the solid $\phi = 0$ phase. This picture economically describes morphological changes deriving from particle–dendrite interactions.

The simulations (see figure 7) show that tip deflection occurs only when the pinning centre is above a critical size, comparable to the dendrite tip radius. Larger pinning centres cause larger deflections. With increasing orientational misfit between the particle and the dendrite, dendrite tip deflection was found to increase. However, above a critical angular difference between the pinning centre and the dendrite ($\Delta\theta \approx 0.35$), the pinning centre is simply engulfed into the dendrite without deflection, while the tip splits to some extent. This is due to the high interface energy at these misorientations, creating an energetic preference for a small layer of liquid around the inclusion. In this case the wet phase boundary appears as a hole in the crystal. An important consequence of this effect is that the angle of tip deflection has an upper limit, thus preventing large deviations from the original growth direction. Pinning centres cause deflection only if *directly* hit by the dendrite tip, a finding confirmed by experiment. This explains the experimental observation that only a small fraction of the pinning centres influence morphology. Using an appropriate density of pinning centres comparable to the density of clay particles, a striking similarity is obtained between experiment and simulation (figure 8). This extends to such details as curling of the main arms and the appearance of extra arms. The disorder in dendrite morphology originates from a polycrystalline structure that develops during a sequential deflection of dendrite tips on foreign particles. With increasing number density of the particles, polycrystals of increasing 'randomness' replace the single-crystal dendrite form, leading to a continuous transition into the *seaweed* morphology (figure 9).

2.6.2. Polycrystalline growth in pure systems and the duality of static and dynamic heterogeneities. The mechanism described above is certainly not a general explanation for polycrystalline growth since spherulites have been observed to grow in liquids without particulates or detectable molecular impurities. How can this be understood? A clue to this phenomenon can be found in the observations of Magill (2001), who noted that spherulites only seem to appear in highly undercooled pure fluids of sufficiently large viscosity. Interpreting Magill's observations, we hypothesize that the decoupling of the translational and rotational diffusion coefficient is responsible for the propensity for polycrystalline growth in highly undercooled liquids. Specifically, a reduced D_{rot} should make it difficult for newly forming crystal regions to reorient with the parent crystal to lower its free energy at the growth front that

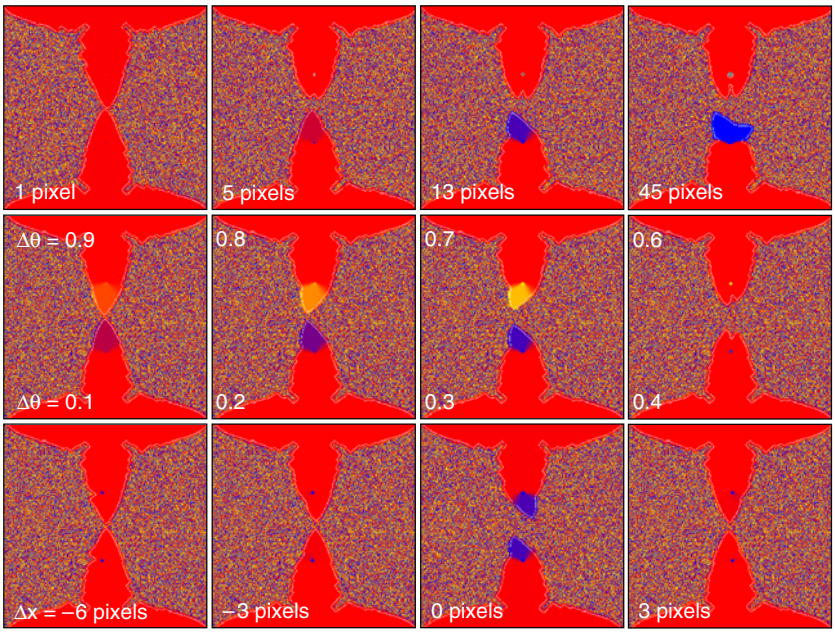

Figure 7. Various influences on the deflection of a dendrite tip by an orientation pinning centre in model B. The first row shows the influence of the size of the pinning centre: larger pinning centres cause larger deflections (the misorientation $\Delta\theta$ is set to 0.333 below and 0.5 above). In the middle row the effect of increasing misorientation $\Delta\theta$ of (13 pixel-sized) pinning centres is shown. As the angle increases beyond 0.3 (or less than 0.7 by symmetry) the effective surface energy increases to the point where the boundary prefers to be 'wet', which results in tip splitting as opposed to deflection. The third row shows that unless the tip is precisely lined up with the (13-pixel) pinning centre, the tip does not deflect, even though the misorientation is $\Delta\theta = 0.3$. Δx is the lateral disposition. (Colouring is the same as for the right panel of figure 5.) The simulations were performed on a 300×300 rectangular grid ($4\ \mu\text{m} \times 4\ \mu\text{m}$), with the thermodynamic properties of Ni–Cu, and 15% anisotropy of the interface free energy. θ is normalized to vary between zero and unity.

is advancing with a velocity scaling with the translational diffusion coefficient. Thus epitaxy cannot keep pace with solidification, i.e., the orientational order that freezes in is incomplete. This situation can be captured within the phase field theory by reducing the orientational mobility while keeping the phase field mobility constant as discussed in detail by Gránásy *et al* (2004).

The first step in this direction has been made by Gránásy *et al* (2003a), who reported the formation of polycrystalline spherulite in model B, when reducing the orientational mobility at large driving force. We recently performed a more systematic study (Gránásy *et al* 2004), which revealed that, as expected, reducing the orientational mobility induces the formation of polycrystalline patterns. Notably, we found similar morphologies and grain structures to those initiated by particulate additives (cf figures 9 and 10). These results indicate a duality between the morphologies evolving due to the effects of static heterogeneities (foreign particles) and dynamic heterogeneities (quenched-in orientational defects).

It is worth noting in this respect that a dendrite to polycrystalline seaweed transition has been observed in electrodeposition (Grier *et al* 1986), and that polycrystalline seaweed structures are commonly observed in electrochemical processes (Fleury 1997) or during the crystallization of electrodeposited layers (Ben-Jacob *et al* 1986, Lereah *et al* 1994). Despite the

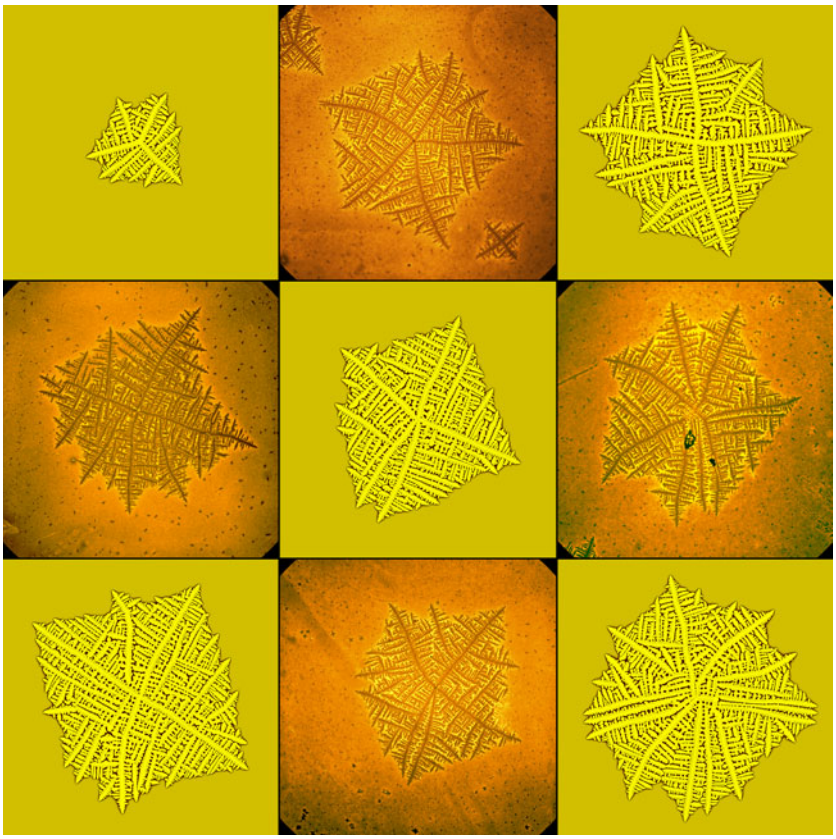

Figure 8. 'Dizzy' dendrites formed by sequential deflection of dendrite tips on foreign particles: comparison of experiments on 80 nm clay–polymer blend film (brown panels, courtesy of V Ferreiro and J F Douglas; for the experimental details see Ferreiro *et al* (2002)) and phase field simulations by model B (yellow panels). The simulations have been selected from 30 simulations according to their resemblance to the experimental patterns. These simulations were performed under identical conditions, except that different initializations of the random number generator have been chosen. (The simulations were performed on a 3000 $\times$ 3000 grid (39.4 μm $\times$ 39.4 μm), with 18 000 single-pixel orientation pinning centres per frame.)

success of modelling fractal-like morphologies on the basis of diffusion-limited aggregation (Vicsek 1989, Halsey 2000), details of the polycrystalline seaweed formation are poorly understood. Quenching of orientational defects into the crystal due to reduced rotational diffusivity under coupling with diffusion controlled fingering (as happens in our phase field model) offers a straightforward explanation for both the morphology and the polycrystalline nature.

2.6.3. From needle crystals to spherulites. One of the popular ideas used to explain the formation of spherulites envisions a regular branching of crystalline filaments with well defined branching angle (see e.g. Keller and Waring 1955, Ryshchenkow and Faivre 1988, Magill 2001). While the details of such a mechanism necessarily differ on the molecular scale for the many systems that display spherulitic solidification, we hope to capture the general features of this process. To incorporate branching with a fixed orientational misfit, we included a new form of the orientational free energy (see model C in the appendix). Here the orientational

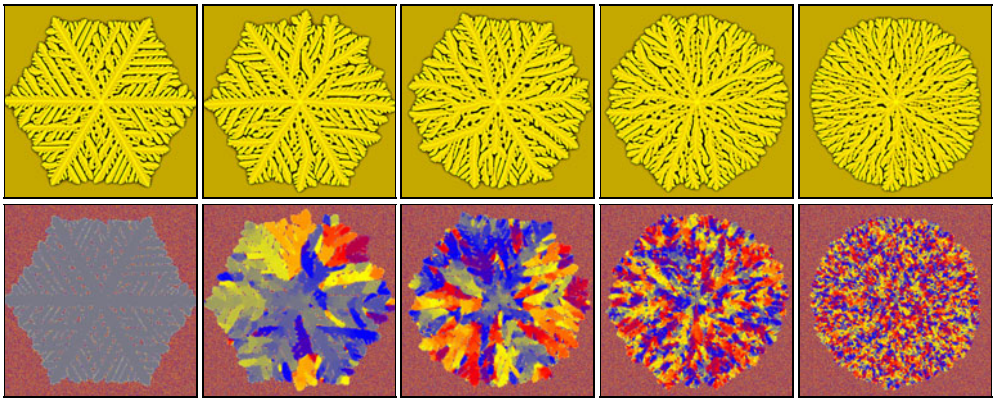

Figure 9. The effect of particulate additives on the growth morphology as predicted by model B. Note the transition from single-crystal dendrite to polycrystalline 'seaweed' structure. Upper row, concentration maps (yellow—solidus, black—liquidus); lower row, orientation maps (colouring is the adaptation of the scheme used in figure 7 for sixfold symmetry). From left to right the numbers of single-pixel orientation pinning centres are $N = 0$, 10 000, 20 000, 50 000, and 100 000, respectively. The interface free energy has a sixfold symmetry and a 2.5% anisotropy. The computations were performed on a 1000 × 1000 grid (13.2 μm × 13.2 μm).

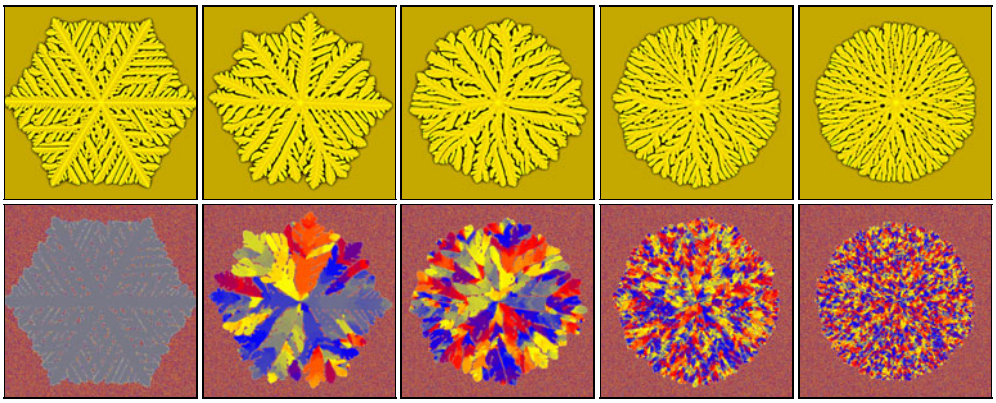

Figure 10. The effect of reduced orientational mobility on the growth morphology. Note the similarity to morphologies shown in figure 9. From left to right the orientational mobility is multiplied by the factors 1, 0.089, 0.08, 0.067, and 0.05, respectively. Other conditions are identical to those for figure 2. (Colouring is the same as for figure 9.)

free energy has a second (local) minimum as a function of misorientation angle $\xi_0|\nabla\theta|$, where ξ_0 is the correlation length of the orientation field. Thus, during orientational ordering at the solid–liquid interface, a second low-free-energy choice (preferred misorientation) is offered. Accordingly, the cells that have a larger misorientation than the first (local) maximum of the f_{ori} versus $\xi_0|\nabla\theta|$ relationship may relax towards the local minimum, unless the orientational noise prevents settling into this local minimum.

The morphologies formed with random 30° branching are shown as a function of supersaturation in figure 11. A large kinetic anisotropy ($\delta_0 = 0.995$) of twofold symmetry is assumed, as this is expected in polymeric systems that have the propensity to form crystal filaments. Otherwise, properties of the familiar Ni–Cu system are used, as many of this system's model parameters are known, and the phase diagram is particularly simple. Ideally,

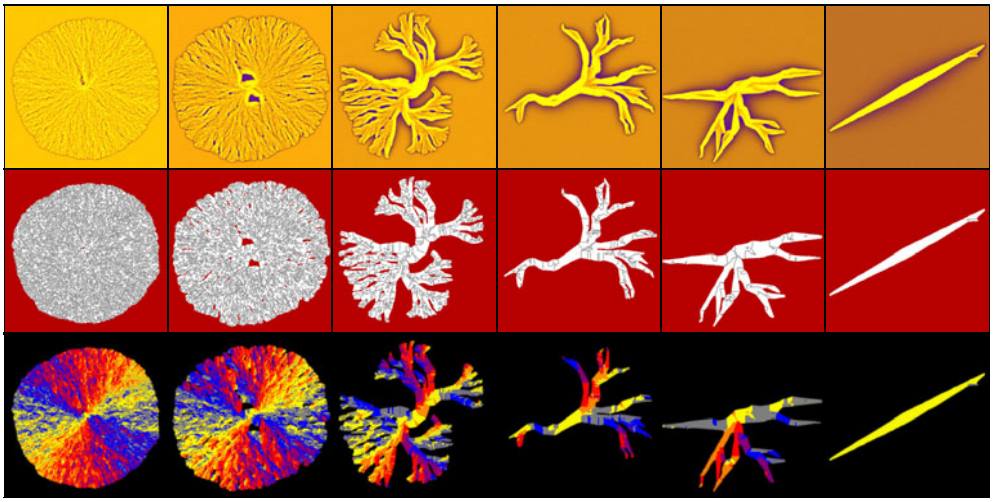

Figure 11. Polycrystalline morphologies formed by random branching with a misfit of 30° in model C. The kinetic coefficient has a twofold symmetry and a large, 99.5%, anisotropy, expected for polymeric substances. Simulations were performed on a 500×500 grid ($6.6\ \mu\text{m} \times 6.6\ \mu\text{m}$). Upper row: composition map (yellow—solidus, dark blue—liquidus). Central row: grain boundary map (grey scale in solid (crystal) shows the local free energy density $HT|\nabla\theta|$). Lower row: orientation map. (The colouring of the orientation map is an adaptation of the scheme shown in previous figures for twofold symmetry: when the fast growth direction is upwards, 60°, or 120° left, the grains are coloured red, blue, or yellow, respectively, while the intermediate angles are denoted by a continuous transition among these colours. Owing to twofold symmetry, orientations that differ by 180° multiples are equivalent.) Unless noise intervenes, six different orientations are allowed, including the orientation of the initial nucleus, which is common for all simulations (30° off horizontal direction (yellow)). In the present colour code, yellow, grey, blue, purple, red, and orange stand for them. In order to make the arms better discernible, in the orientation map, the liquid (which has random orientation, pixel by pixel) has been coloured black. The supersaturation varies from left to right as $S = 1.1$, 1.0, 0.95, 0.90, and 0.75. Note the chain of transitions that links the needle crystal forming at low supersaturation to 'axialites', crystal 'sheaves', and eventually to the spherulites (with and without 'eyes'—uncrystallized holes—on the two sides of the nucleus).

in a system where filament branching happens with a 30° misfit, the polycrystalline growth form may consist of only grains that have six well defined orientations (including the one that nucleated), which differ by multiples of 30°. Indeed this is observed, with some noise driven faults at high driving forces. At low supersaturations, needle crystals form. With increasing driving force, the branching frequency increases, and more space filling patterns emerge, while the average grain size decreases. This leads to a continuous morphological transition that links the needle crystals forming at low supersaturation to axialites, to crystal sheaves, and eventually to spherulites (with and without 'eyes' on the two sides of the nucleus) that form far from equilibrium.

A sequence of snapshots shows the birth of a spherulite (figure 12). First crystal 'sheaves' of diverging ends form, that spread with time more and more, forming finally a spherulite with two 'eyes'—uncrystallized holes—on the sides of the nucleus, a pattern common in polymeric systems (see e.g. Magill 2001).

Other prominent polycrystalline growth forms are presented in figure 13. Rare branching with low misfit (e.g., 15°) and low driving force leads to the formation of arboresque structures (see the 'willow tree'-like pattern in figure 13). A pattern resembling 'quadrites' has been obtained with dense perpendicular branching. If the metastable free energy well is deep, and

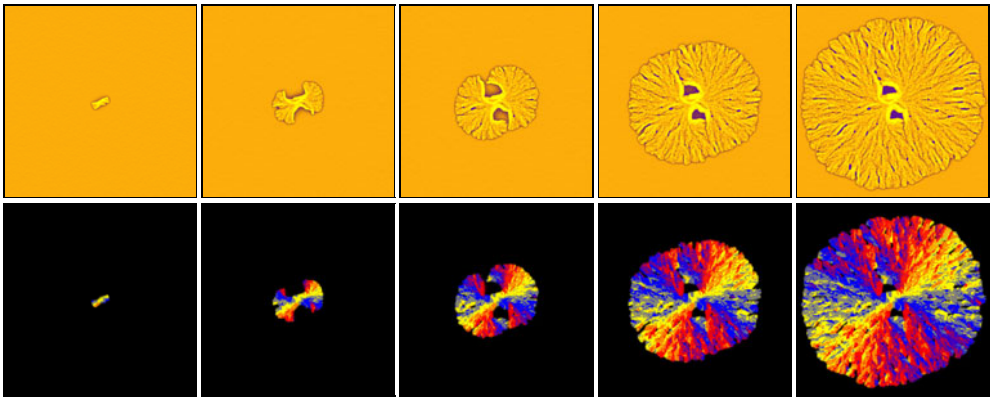

Figure 12. The birth of a spherulite at $S = 1.0$, as predicted by model C. Time increases from left to right. Upper row, composition map; lower row, orientation map.

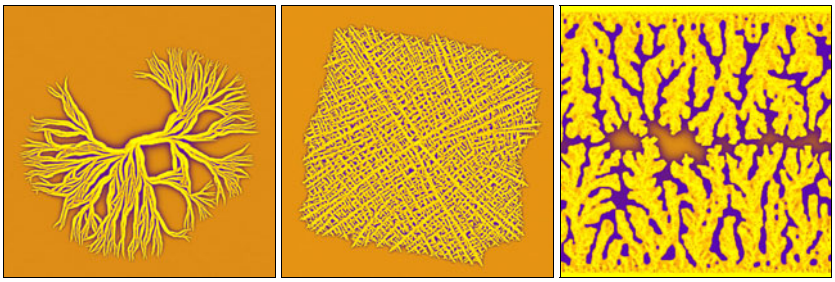

Figure 13. Polycrystalline growth morphologies as predicted by model C: arboresque spherulite obtained with a branching angle of 15°, on a 2000 × 2000 grid (26.3 μm × 26.3 μm) (cf figure 1(f)); 'quadrite'-like growth form obtained with a branching angle of 90°, on a 2000 × 2000 grid (26.3 μm × 26.3 μm) (cf figure 1(h)); and fractal-like aggregates obtained with a branching angle of 60°, on a 500 × 500 grid (6.6 μm × 6.6 μm) (cf figure 1(i)).

the driving force is not too large, copious nucleation of new grains occurs at the interface, leading to essentially isotropic fingering, yielding polycrystalline fractal-like structures.

Work is underway to map the zoo of possible polycrystalline morphologies. While the similarity of the simulations and the experimental patterns is reassuring, further experimental work is also needed to determine whether the predicted grain structures are indeed realistic.

2.6.4. Eutectic spherulites with locked orientational misfit. In some of the eutectic systems, the two solid phases are expected to have a well defined orientational relationship. Pusztai and Gránásy modified model B to address such a situation: regular solution thermodynamics has been built in, and a free energy term has been added that prefers a fixed misorientation at the phase boundaries (see Lewis *et al* 2004). Since the model contains a single structural order parameter (phase field), it is strictly applicable only to systems where the two phases have the same crystal structure (e.g., Ag–Cu, Ag–Pt). Simulations have been performed for the Ag–Cu system at three compositions (hypo-eutectic, eutectic, and hyper-eutectic), which showed that the model successfully accounts for orientational locking of the solid phases (figure 14).

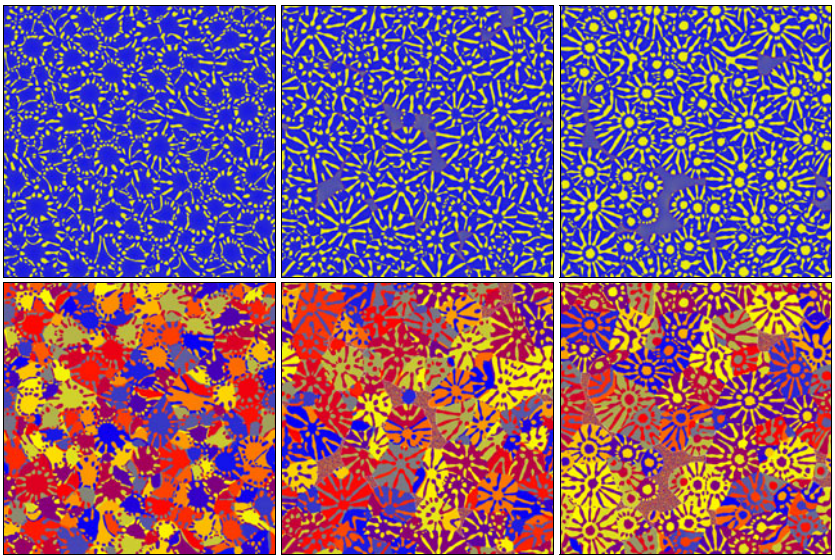

Figure 14. Equiaxed solidification in hypo-eutectic ($c_{Cu} = 0.3$), eutectic ($c_{Cu} = 0.35$), and hyper-eutectic ($c_{Cu} = 0.4$) Ag–Cu liquids at 900 K as predicted by the phase field theory. Composition maps are shown in the top row; the respective orientation maps are in the bottom row. (Colouring: in the composition maps, continuous change from blue to yellow indicates compositions varying from $c_{Cu} = 0$ to 1, respectively. In the orientation maps, different colours stand for different crystallographic orientations in the laboratory frame.) Note the locked (fixed) misorientation of the two phases within the eutectic particles.

2.7. Grain boundaries

Phase field modelling of grain boundaries themselves is a natural subset of the above treatment, with only a few modifications to the controlling equations of motion. All of the processes addressed in this paper, so far, address the *formation*, of a polycrystalline material, and thus yield systems with intricate grain networks. However, none of these treatments examines the subsequent evolution of the grain structure in the largely solid final state. This is, of course, quite reasonable, as the timescales associated with grain boundary dynamics are typically far slower than the speeds associated with any of the solidification phenomena addressed herein. Thus, all processes in the solid are approximately 'frozen in' within the confines of our model.

However, using the equations developed in the appendix treatment of model A, we are able to describe the formation of a foam-like multi-grain structure by impingement of solidifying grains and the subsequent evolution of this grain network. These types of simulations have been done before using models described in section 2.2, but the present approach has all of the advantages detailed in the other sections, while still being able to describe foam-like grain structures. As is detailed in the appendix, within model A, grain boundaries can be made mobile if a higher-order term, $|\nabla\theta|^2$, is present in the free energy. This term renders the 'jump' in θ continuous in its derivative ($|\nabla\theta|$ remains finite). This, in turn, numerically unpins the boundary. Additionally, the presence of dynamics in θ implies the possibility of grain rotation, admitting another means by which the grain network can lower its free energy.

As a consequence of this mobility, the grain boundaries are now able to readjust their configuration after impingement to find a lower-energy state. Often this state is characterized by grain boundary wetting, a phenomenon commonly observed in materials systems. There have been substantial experimental and theoretical studies of the grain wetting phenomenon

(Glicksman and Vold 1969, Blendell *et al* 1999, Chatain *et al* 2001). We should note that characterization of wetting away from the melting point is more ambiguous because the liquid/solid interface can only be stabilized by curvature (through the Gibbs–Thomson effect); however, the numerical simulations shown below exhibit behaviour that is consistent with rudimentary expectations. In general, a system with variable composition will have a variable melting point and this is expected to elucidate additional aspects of wetting phenomena (Rappaz *et al* 2003). However, while one can consider the binary alloy case, it is instructive in this instance to examine the theory in the case of pure (single-component) material. The approach detailed here closely follows the arguments made by Warren *et al* (2003a).

2.7.1. Grain boundary wetting. Because the model contains both a cost for the presence of a grain boundary and the ability to model a liquid–solid interface, a transition from the classical limit of a 'dry' grain boundary to a wet boundary is possible. A simple energetic argument suggests that if the grain boundary energy should rise to more than twice the liquid–solid surface energy, then the system would prefer to contain two liquid–solid interfaces, and the boundary will wet. We examine our model in the case where $T = T_{\mathrm{m}}$, the melting temperature of the material, and examine the case where the coefficient of the $|\nabla\theta|^2$ term $\varepsilon_\theta = 0$, as we do not need grain boundary mobility for this mathematical argument (although we will reintroduce it for the simulations). The value of the phase field at a bi-crystal interface between two grains differing by a misorientation of $\Delta\theta$ is termed $\phi_{\max}$ and has a value

$$\phi_{\max} = \frac{H\,\Delta\theta}{a\varepsilon_\phi} = \frac{\Delta\theta}{\Delta\theta_{\mathrm{c}}^*}$$

where $\Delta\theta_{\mathrm{c}}^* \equiv a\varepsilon_\phi/H$, and a is related to the height of the free energy barrier between the solid and liquid states in equilibrium. For convenience, let us define the value $\phi_* \equiv 1 - \phi_{\max}$. If $\Delta\theta > \Delta\theta_{\mathrm{c}}^*$, there is no stationary solution to the bi-crystal problem (at the melting point), and the boundary will melt above this angle. The width of the boundary d is found to be

$$d = -\frac{2\varepsilon_\phi}{a}\ln\phi_* = -\frac{2\varepsilon_\phi}{a}\ln\left(1 - \frac{\Delta\theta}{\Delta\theta_{\mathrm{c}}^*}\right),$$

which diverges logarithmically as $\Delta\theta \to \Delta\theta_{\mathrm{c}}^*$ from below. Another perspective on the meaning of the critical angle $\Delta\theta_{\mathrm{c}}^*$ can be obtained by computing, when $T = T_{\mathrm{m}}$, the bi-crystal boundary energy

$$\gamma_{\mathrm{bc}} = s\Delta\theta\phi_*^2 - a\varepsilon_\phi\phi_*^2\left(1 - \frac{2\phi_*}{3}\right) + \frac{a\varepsilon_\phi}{3} = \frac{a\varepsilon_\phi}{3}\left(1 - \phi_*^3\right).$$

We carefully have not asserted that γ_{bc} is the grain boundary energy γ_{gb}. In actuality, γ_{bc} is the excess energy due to the misorientation of two grains of crystal, which encompasses three classical quantities: liquid–solid surface energy, grain boundary energy, and the energy of any undercooled intervening liquid phase. We wish to compare this energy with the liquid–solid surface energy. The mathematics for the liquid–solid interface solution to this phase field model is nearly identical to the bi-crystal case. For the liquid–solid case $\Delta\theta = 0$, and thus there is no step-function in the θ profile. The surface energy of the isolated liquid–solid interface in this model is

$$\gamma_{\mathrm{ls}} = \varepsilon_\phi\int_0^1 \mathrm{d}\phi\,\sqrt{2f} = \frac{a\varepsilon_\phi}{6}.$$

The bi-crystal energy can therefore be re-expressed as

$$\gamma_{\mathrm{bc}} = 2\gamma_{\mathrm{ls}}(1 - \phi_{\min}^3) \leqslant 2\gamma_{\mathrm{ls}}.$$

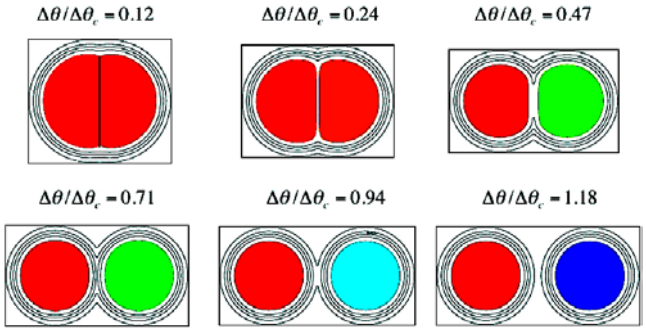

Figure 15. Co-existing (metastable) crystallite pairs, as a function of misorientation relative to the critical misorientation. Note the formation of a wet grain boundary as $\Delta\theta \rightarrow \Delta\theta_c$. The black lines are the phase field contours from 0.1 to 0.9 in steps of 0.2, while the colours represent orientation (rainbow colour map).

Thus, at the melting temperature, the boundary energy rises to $2\gamma_{ls}$ as $\Delta\theta$ increases to $\Delta\theta_c^*$. At $\Delta\theta = \Delta\theta_c^*$, the boundary melts (infinite width). This is referred to as grain boundary wetting or grain boundary melting, and the critical angle is defined by $\gamma_{bc}(\Delta\theta_c^*) = 2\gamma_{ls}$. Note also that if $\Delta\theta_c^*$ is greater than the largest possible misorientation then the boundary will never melt, and all boundaries will be dry in equilibrium at the melting temperature. As expected, all of this analysis carries over to the $\varepsilon_\theta \neq 0$ case, albeit without the analytic transparency which was the motivation for this section's treatment of the problem. Having detailed the mathematics of grain boundary wetting, we can perform simulations of two abutting drops of differing orientation equilibrating in an undercooled melt. If we numerically prohibit the drops from undergoing coarsening (which will cause one to shrink and one to grow) we can examine the metastable state where both drops co-exist for all time (figure 15). As we can see, as $\Delta\theta$ increases to $\Delta\theta_c$ the drops separate, and the boundary wets.

2.7.2. Grain impingement and coarsening. Having studied some of the steady state properties of grain boundaries within our model, we can now perform larger-scale simulations, which ultimately evolve like a two-dimensional foam. In figure 16 (upper row) we show an isothermal two-dimensional simulation of the full model, with many nuclei introduced simultaneously into an undercooled melt. (Details of the simulation are given by Warren *et al* (2003a).) The grains impinge and then coarsening occurs, all within the same governing equations. All of the dynamics discussed above, except grain rotation, are in evidence: (i) solidification, (ii) grain boundary formation (iii) and grain coarsening. Grain rotation is suppressed with our parameter choices. The relative dominance of rotation versus grain boundary motion can also be investigated, by separately controlling the timescales for each phenomenon. In figure 16 (lower row), rotation dominated relaxation of the microstructure is shown. Note that grain rotation in the solid phase is a phenomenon relevant to nanocrystals.

2.8. Effect of walls

Solidification in the presence of walls is of great practical importance. In casting, solidification usually starts by heterogeneous crystal nucleation on the walls of the mould (e.g. Kurz and Fisher 1989). With the exception of extremely pure samples, even volume nucleation happens mostly via a heterogeneous mechanism (on the surface of floating foreign particles) (Turnbull 1952). Particulate additives are widely used as grain refiners, to reduce grain size by enhancing

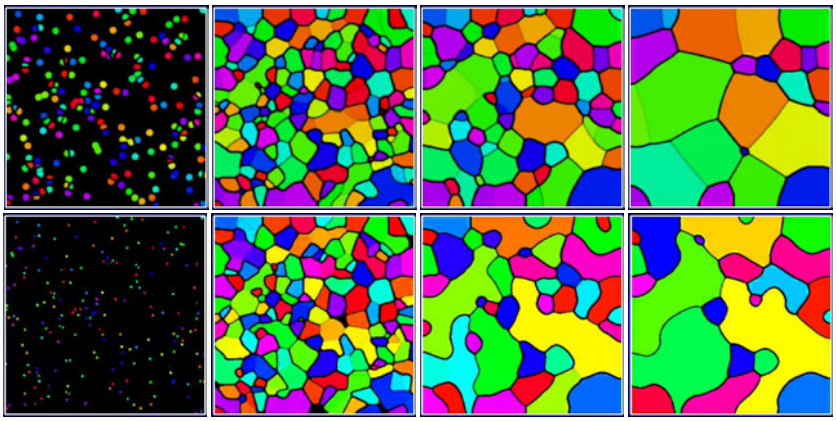

Figure 16. Grain boundary relaxation in model A. Time increases from left to right. Upper row: grain impingement and boundary evolution dominated by grain boundary migration. Lower row: evolution dominated by grain rotation. (M_θ is reduced by 100 from the upper row.) Different colours denote different grain orientations.

the nucleation rate. Nonetheless, heterogeneous nucleation is probably the only stage of solidification where the micro-mechanism of the process is largely unknown. While the phase field method has been used to address problems that incorporate heterogeneous nucleation, this process is usually mimicked introducing supercritical particles into the simulation window (Lo *et al* 2001, 2003). Recently, however, steps have been made towards a physical modelling of heterogeneous nucleation within the phase field theory. Castro (2003) introduced walls into a single-order-parameter theory by assuming a no-flux boundary condition at the interface ($\mathbf{n}\nabla\phi = 0$, where $\mathbf{n}$ is the normal vector of the wall), which results in a contact angle of 90° at the wall–solid–liquid triple junction. Langevin noise is then introduced to model nucleation. It has been found that the presence of walls enhances nucleation, and thus the internal corners are places where nucleation is more likely to occur.

Prescribing $(\mathbf{n}\nabla\phi) = 0$ and $(\mathbf{n}\nabla c) = 0$ at the wall perimeter, we introduced chemically inert surfaces into model B, and performed simulations to address heterogeneous volume nucleation on foreign particles (a more detailed description than the 'pinning centres'), on rough surfaces, and in confined space (porous matter and channels). A few preliminary results, which illustrate that various complex phenomena can be addressed this way, are shown in figure 17. Further work will explore the kinetics of these processes, and extend the modelling to arbitrary contact angles.

3. Summary and future directions

In the previous section we demonstrated the capability of the phase field method to describe complex polycrystalline morphologies. This includes nucleation and growth problems in anisotropic systems, the effect of particulate additives and trapped disorder on growth morphologies, solidification in confined space, and many others. However, systematic studies are needed on all areas discussed here (e.g., mapping of possible morphologies, study of transformation kinetics in the presence of walls, etc). Of particular interest to us is the validation of the models that include random branching. This requires the collection of statistics on the morphologies both in theory and experiment, as these patterns may have only statistical similarity. Straightforward extensions of the work performed with models

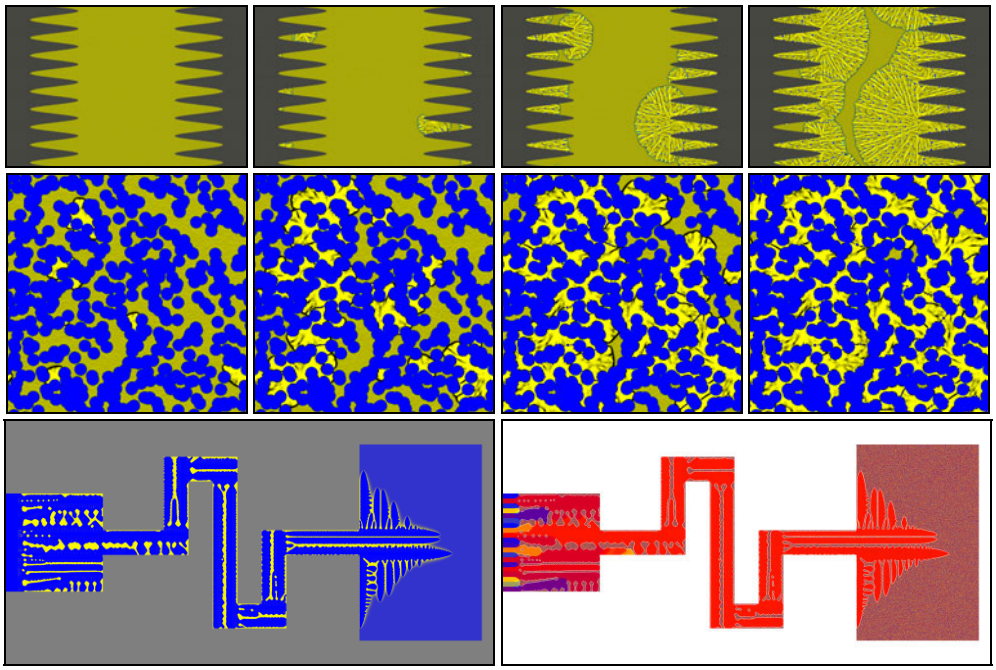

Figure 17. Solidification in the presence of walls/particles in model B. Upper row: heterogeneous nucleation on rough surfaces (walls are grey). Central row: heterogeneous nucleation and crystallization in porous matter (blue—particles of porous matter, bright yellow—crystal, khaki—liquid). Note that nucleation happens in the notches between particles of the porous matter. Bottom row: dendritic solidification in a two-dimensional orientation selector (pigtail) mimicking the casting of single-crystal components. Left, composition field (blue—solidus, yellow—liquidus, grey—mould); right, orientation field (colouring is the same as in the right panel of figure 5, white—mould). Crystallization starts on the left with several crystallographic orientations, but only a single crystallographic orientation survives the meandering channel to reach the volume on the right.

B and C may include coupling to hydrodynamics (an essential step to study particle–front interaction), and dynamically changing temperatures. The largest theoretical challenge is perhaps the generalization of the model to three dimensions. This requires three orientational fields (e.g., two polar angles that set the fast growth direction in 3D, and a third angle that specifies the rotation of the crystal around this axis). The simple model of elasticity that these models inherently contain should be refined using the continuously developing inventory of phase field models for solid-state transformations (e.g., Khachaturyan 1983, Wen *et al* 1999, Löchte *et al* 2000, Artemev *et al* 2000, Wang *et al* 2003). The broad interface remains an issue (enhanced solute trapping, etc). New approaches (e.g. Amberg 2004) should address some of the numerical issues associated with too thick interfaces, while interaction with atomistic scale modelling will help to fix the model parameters for quantitative calculations.

Regarding future directions, we mention a most remarkable new approach to polycrystalline solidifications: a new field theory by Elder *et al* (2002) that allows for atomistic modelling of the solid–liquid transition on diffusive timescales. A negative square-gradient term is balanced here by a positive fourth-order term, yielding homogeneous (liquid) regions and crystalline (‘dots’ on lattice) regions in the phase diagram, with a first-order phase transition in between. The model naturally incorporates crystal anisotropy, elastic and

plastic deformations, grain boundaries, cracks, epitaxy, etc (Elder and Grant 2004). Its results are consistent with the Read–Shockley theory of grain boundary energy and the Matthews–Blakeslee theory for misfit dislocations in epitaxy. The model has been applied for eutectic solidification and dendritic growth (Elder 2004). With the ever-increasing power of computers, this approach is expected to take over many of the tasks of the phase field theory.

Summarizing, the authors believe that, in the foreseeable future, phase field theories, and field theoretic methods in general, will be among the most powerful tools of computational materials science.

Acknowledgments

The authors are indebted to J F Douglas for the illuminating discussions on polycrystalline solidification. We thank V Ferreiro and J F Douglas for the images of transformation in polymer thin films, V Fleury for the picture of the electrodeposited patterns, and G Faivre for the image of the Se spherulite. LG is grateful for extensive discussions on the phase field theory to M Plapp and T Börzsönyi, and to T Börzsönyi for his contributions to the numerical implementation/development of model B. JAW would also like to acknowledge his collaborators and intellectual partners in developing model A: W C Carter, R Kobayashi, and A E Lobkovsky, as well as W J Boettinger, J W Cahn, R E Garcia, J Guyer, G B McFadden, R F Sekerka, and D Wheeler for many discussions on various aspects of the research. This work has been supported by contracts OTKA-T-037323 and ESA PECS Contract No 98005, and by the EU Integrated Project IMPRESS, and forms part of ESA MAP Projects Nos AO-99-101 and AO-99-114. TP acknowledges support by the Bolyai János Scholarship of the Hungarian Academy of Sciences.

Appendix. Phase field models used in preparing the illustrations

We specify here three models (models A, B, and C), which show rather similar features; however, they differ in important details such as the form of the free energy functional. *Note that the models termed here as models A–C differ from models A–C of the usual* Hohenberg and Halperin (1977) *classification.* Once the free energy functional is defined, the equations of motion for the three fields are obtained as follows.

$$\dot{\phi} = -M_\phi \frac{\delta F}{\delta \phi} = M_\phi \left\{ \nabla \left(\frac{\partial f}{\partial \nabla \phi} \right) - \frac{\partial f}{\partial \phi} \right\} + \zeta_\phi$$

$$\dot{c} = \nabla M_c \nabla \frac{\delta F}{\delta c} = \nabla \left\{ Dc(1-c)\nabla \left[\left(\frac{\partial f}{\partial c} \right) - \nabla \left(\frac{\partial f}{\partial \nabla c} \right) \right] \right\} + \zeta_j$$

$$\dot{\theta} = -M_\theta \frac{\delta F}{\delta \theta} = M_\theta \left\{ \nabla \left(\frac{\partial f}{\partial \nabla \theta} \right) - \frac{\partial f}{\partial \theta} \right\} + \zeta_\theta$$

where M_i and ζ_i stand for the appropriate mobilities and Langevin-noise terms.

A.1. Model A by Warren et al (2003a)

We start with the free energy for the model of Warren *et al* (2003a):

$$F = \int \mathrm{d}^3 r \left\{ \frac{\varepsilon_\phi^2}{2} s^2(\vartheta - \theta) |\nabla \phi|^2 + \frac{\varepsilon_\theta^2}{2} \eta(\phi) |\nabla \theta|^2 + H \lambda(\phi) |\nabla \theta| + f(\phi, T) \right\} \tag{A.1}$$

where H and ε_θ specify the strength of the coupling between ϕ and $\nabla\theta$, while $\lambda(\phi)$ and $\eta(\phi)$ are as yet unspecified, monotonically increasing functions of ϕ. The monotonic nature of $\lambda(\phi)$

and $\eta(\phi)$ is required if the effects of crystal orientation are to be reduced or eliminated in the liquid phase. In what follows we take $\lambda(\phi) = \eta(\phi) = 1-\phi^2$. The free energy density $f(\phi, T)$ is a double well in ϕ, with a bias favouring the solid or liquid phase depending on whether the temperature is below or above the melting point of the material. The relation of the remainder of the parameters to more familiar quantities, as well as the specific form of $f(\phi, T)$ is made more explicit in the section on model B, below.

With the removal of the terms in the free energy density in the integrand of equation (A.1) that depend on the orientation, this model reduces to a simple phase field model of solidification. The presence of the linear term $|\nabla\theta|$ (as opposed to higher-order powers in $|\nabla\theta|$) is required for grain boundaries that are localized at equilibrium; without this linear term the grain boundary regions (where θ is spatially varying) spread without bound by relaxational dynamics. In other words, stable grain boundaries of finite width do not exist in the model unless the free energy density depends, to lowest order, linearly on $|\nabla\theta|$ (Kobayashi *et al* 2000). The linear dependence on $|\nabla\theta|$ introduces a cusp into the total free energy density at $\nabla\theta = 0$. In addition to the linear term, we include $|\nabla\theta|^2$. At least one term of higher order than linear is essential for the dynamics to include grain boundary motion (Kobayashi *et al* 2000, Lobkovsky and Warren 2001). As stated above, the dynamics of the system are relaxational, and we choose to consider a pure material. This allows us to eliminate the concentration equation, but, if we choose to look at non-isothermal systems, we then require a proper accounting of heat flow. Using arguments of entropy production, one can develop self-consistent equations for all the thermodynamic variables (Wang *et al* 1993). However, it is straightforward to write out the phenomenological equation for temperature directly. The evolution equation for the time-dependent temperature, T, is

$$\frac{\partial T}{\partial t} = D_{\mathrm{T}}\nabla^2 T + \frac{L}{c}\frac{\partial \phi}{\partial t},$$

where L is here the latent heat of freezing and c is the specific heat, and D_{T} is the thermal diffusivity.

Applying the above relaxation hypothesis yields the following two equations for the phase field ϕ and orientation field θ:

$$\begin{aligned} \frac{\partial \phi}{\partial t} &= M_\phi\left[\varepsilon_\phi^2\nabla^2\phi - \frac{\partial f}{\partial \phi} - 2H\phi|\nabla\theta| - \varepsilon_\theta^2\phi|\nabla\theta|^2\right] \\ P(|\nabla\theta|)\phi^2\frac{\partial \theta}{\partial t} &= M_\theta\left\{\nabla\left[\phi^2\left(\frac{H}{|\nabla\theta|} + \varepsilon_\theta^2\right)\nabla\theta\right]\right\}, \end{aligned} \tag{A.2}$$

where we have introduced the function P to control the kinetics of the angle variable in grain and grain boundary regions by choosing

$$P(\varepsilon_\theta|\nabla\theta|) \qquad \text{with } P(w) = 1 - \mathrm{e}^{-\beta w} + \frac{\mu}{\varepsilon_\theta}\mathrm{e}^{-\beta w}.$$

The parameters β and μ are introduced to separately control the mobility of grain boundaries (β) and the rotation rate of grains (μ). Note that all parameters appearing in equations (A.2) are non-dimensionalized in the following manner:

$$\begin{aligned} &\varepsilon_\theta = al_0\tilde{\varepsilon}_\theta; \qquad \varepsilon_\phi = al_0\tilde{\varepsilon}_\phi; \qquad H = al_0^2\tilde{H}; \qquad M_\phi = M_\phi/a^2t_0; \\ &M_\theta = M_\theta/a^2t_0; \qquad \mathbf{r} = (x, y, z) = (l_0\tilde{x}, l_0\tilde{y}, l_0\tilde{z}) \end{aligned}$$

where tildes indicates dimensionless parameters, a^2 is eight times the height of the energy barrier between liquid and solid at the melting point, and l_0 and t_0 are convenient length and timescales, respectively. The solution of these equations requires some care, and the interested readers are referred to Warren *et al* (2003a).

A.2. Model B by Gránásy et al (2002a, 2002b)

This model builds on earlier results by Warren and Boettinger (1995) and Kobayashi *et al* (1998).

The *free energy functional* is

$$F = \int \mathrm{d}^3 r \left\{ \frac{\varepsilon_\phi^2 T}{2} s^2(\vartheta - \theta)|\nabla\phi|^2 + \frac{\varepsilon_c^2 T}{2}|\nabla c|^2 + w(c) T g(\phi) + [1 - p(\phi)][f_S(c, T) + f_{\mathrm{ori}}(|\nabla\theta|)] + p(\phi) f_L(c, T) \right\},$$

where

$$\varepsilon_\phi^2 = \frac{6\sqrt{2}\gamma_{\mathrm{A,B}}\delta_{\mathrm{A,B}}}{T_{\mathrm{A,B}}}, \qquad w(c) = (1-c)w_{\mathrm{A}} + c w_{\mathrm{B}}, \qquad w_{\mathrm{A,B}} = \frac{12\gamma_{\mathrm{A,B}}}{\sqrt{2}\delta_{\mathrm{A,B}} T_{\mathrm{A,B}}},$$

$$g(\phi) = \tfrac{1}{4}\phi^2(1-\phi)^2, \qquad g'(\phi) = \phi^3 - \tfrac{3}{2}\phi^2 + \tfrac{1}{2}\phi$$

$$p(\phi) = \phi^3(10 - 15\phi + 6\phi^2), \qquad p'(\phi) = 30\phi^2(1-\phi)^2,$$

$$f_{\mathrm{ori}} = HT|\nabla\theta|$$

$$s(\vartheta - \theta) = 1 + s_0 \cos(m\vartheta - 2\pi\theta), \qquad \vartheta = \arctan[(\nabla\phi)_y/(\nabla\phi)_x].$$

Here ε_ϕ and ε_c are the coefficients of the square-gradient term for the fields ϕ and c; w_i is the free energy scale for the ith pure component ($i = A, B$); s, g and p are the anisotropy function, the quartic double-well function and the interpolation function. γ_i, δ_i, and T_i are the interface free energy, interface thickness, and melting point for the ith pure component ($i = A, B$). ϑ is the inclination of the normal vector of the interface in the laboratory frame. H determines the free energy of the low-angle grain boundaries. s_0 is the amplitude of the anisotropy of the interface free energy, while m is the symmetry index ($m = 6$ for sixfold symmetry).

The dimensionless form of the deterministic part of the equations of motion has been obtained by multiplying the original equations by ξ^2/D_l, where ξ is a convenient length scale used for de-dimensionalizing, and D_l is the diffusion coefficient in the liquid.

(a) *Phase field:*

$$\tilde{\dot{\phi}} = \frac{M_\phi \varepsilon_\phi^2 T}{D_l}\left[\tilde{\nabla}(s^2\tilde{\nabla}\phi) - \frac{\partial}{\partial\tilde{x}}\left\{s\frac{\partial s}{\partial\vartheta}\frac{\partial\phi}{\partial\tilde{y}}\right\} + \frac{\partial}{\partial\tilde{y}}\left\{s\frac{\partial s}{\partial\vartheta}\frac{\partial\phi}{\partial\tilde{x}}\right\} - \xi^2\frac{w(c)Tg'(\phi) + p'(\phi)\{f_L(c,T) - f_S(c,T) - f_{\mathrm{ori}}(|\nabla\theta|)\}}{\varepsilon_\phi^2 T}\right].$$

(b) *Concentration field:*

$$\tilde{\dot{c}} = \tilde{\nabla}\left\{\frac{v_m}{RT}\lambda c(1-c)\tilde{\nabla}\left[(w_{\mathrm{B}} - w_{\mathrm{A}})Tg(\phi) + [1-p(\phi)]\frac{\partial f_S}{\partial c}(c,T) + p(\phi)\frac{\partial f_L}{\partial c}(c,T) - \frac{\varepsilon_c^2 T}{\xi^2}\tilde{\nabla}^2 c\right]\right\}.$$

(c) *Orientation field:*

$$\tilde{\dot{\theta}} = \chi\left[\tilde{\nabla}\left\{[1-p(\phi)]\frac{\tilde{\nabla}\theta}{|\tilde{\nabla}\theta|}\right\} - \frac{\varepsilon_\phi^2}{H\xi}s\frac{\partial s}{\partial\theta}|\tilde{\nabla}\phi|^2\right].$$

Here quantities with tildes are dimensionless. The phase field mobility can be anisotropic, $M_\phi = M_{\phi,0}\{1 + \delta_0\cos[m(\vartheta - \theta)]\}$, where $M_{\phi,0}$ is the average value of the phase field

mobility and δ_0 is the amplitude of the anisotropy. The concentration equation has been obtained using $M_c = (v_m/RT)Dc(1-c)$ as the mobility of the concentration field, where v_m is the average molar volume, and $D = D_s + (D_l - D_s)p(\phi)$ is the diffusion coefficient, D_s the diffusion coefficient in the solid, while $\lambda = D/D_l$ the reduced diffusion coefficient. In the last equation, $\chi = M_\theta \xi HT/D_l$ is the dimensionless orientational mobility, while $M_\theta = M_{\theta,s} + (M_{\theta,l} - M_{\theta,s})p(\phi)$.

The stochastic part of the equations of motion: Gaussian noises of amplitude $\zeta = \zeta_s + (\zeta_l - \zeta_s)p(\phi)$ are added to the non-conserved fields, where ζ_l and ζ_s are the amplitudes in the liquid and solid, while in the case of the conserved concentration field, random concentration fluxes are added to the equation of motion.

Remarks:

(i) The second term in the equation for orientation field requires some care. It is negligible if the physical interface thickness ($\sim$1 nm) is used. When, due to limitations of computer power, a broad interface is used, it leads to artefacts. To avoid this difficulty in the simulations, we adopt one of the following measures: (a) perform the calculations in the presence of only kinetic anisotropy (then this term is zero); (b) we omit this term.

(ii) The governing equations have been solved numerically using an explicit finite difference scheme. Unless stated otherwise periodic boundary conditions were used. Stable solution of the orientational equation needs about 1/20 of the time step required for the stable solution of the other fields. A parallel code has been developed that relies on the message passing interface (MPI) protocol and was run on a PC cluster consisting of 75 nodes and a server machine.

A.3. Model C (Gránásy and Pusztai 2004)

This differs from model B in that a new form of the orientational free energy is assumed:

$$f_{\mathrm{ori}} = \frac{HT}{2\xi_0}\{x F_0 + (1-x)F_1\}$$

$$F_0 = \begin{cases} |\sin(2\pi m \xi_0 |\nabla\theta|)| & \text{for } \xi_0|\nabla\theta| < \frac{3}{4m} \\ 1 & \text{otherwise} \end{cases}$$

$$F_1 = \begin{cases} |\sin(2\pi n \xi_0 |\nabla\theta|)| & \text{for } \xi_0|\nabla\theta| < \frac{1}{4n} \\ 1 & \text{otherwise} \end{cases}$$

where the free energy of small-angle grain boundaries scales with HT; $\xi_0 = \Delta x$ is the correlation length of the orientation field. Note that F_0 has a minimum at $\xi_0|\nabla\theta| = 1/2m$, and saturates at $\xi_0|\nabla\theta| = 3/4m$; while F_1 increases monotonically, and saturates at $\xi_0|\nabla\theta| = 1/4n$. Thus f_{ori} has minima at $\xi_0|\nabla\theta| = 0$ (absolute) and $1/2m$ (local); i.e., m determines the branching angle. In the computations $n = 1/2$ has been set.

While the equations of motion for the phase field and concentration remain unchanged (only the actual f_{ori} has to be inserted into the former), the deterministic part of the equation of motion for the orientation field takes the following form:

$$\dot{\tilde{\theta}} = \chi\left[\tilde{\nabla}\left\{[1-p(\phi)]\pi[x\tilde{F}_0 m + (1-x)\tilde{F}_1 n]\frac{\tilde{\nabla}\theta}{|\tilde{\nabla}\theta|}\right\} - \frac{\varepsilon_\phi^2}{H\xi}s\frac{\partial s}{\partial\theta}|\tilde{\nabla}\phi|^2\right]$$

where

$$\tilde{F}_0 = \begin{cases} \mathrm{sgn}[\sin(2\pi m\tilde{\xi}_0|\tilde{\nabla}\theta|)]\cos(2\pi m\tilde{\xi}_0|\tilde{\nabla}\theta|) & \text{for } \tilde{\xi}_0|\tilde{\nabla}\theta| < \frac{3}{4m} \\ 0 & \text{otherwise} \end{cases}$$

$$\tilde{F}_1 = \begin{cases} \mathrm{sgn}[\sin(2\pi n\tilde{\xi}_0|\tilde{\nabla}\theta|)]\cos(2\pi n\tilde{\xi}_0|\tilde{\nabla}\theta|) & \text{for } \tilde{\xi}_0|\tilde{\nabla}\theta| < \frac{1}{4n} \\ 0 & \text{otherwise} \end{cases}$$

while $\tilde{\xi}_0 = \xi_0/\xi$.

References

Amberg G 2004 *Phys. Rev. Lett.* **91** 265505
Apel M, Boettger B, Diepers H J and Steinbach I 2002 *J. Cryst. Growth* **237** 154–8
Artemev A, Wang Y and Khachaturyan A G 2000 *Acta Mater.* **48** 2503–18
Auer S and Frenkel D 2001a *Nature* **409** 1020–3
Auer S and Frenkel D 2001b *Nature* **413** 711–3
Báez L A and Clancy P 1995 *J. Chem. Phys.* **102** 8138–48
Ben-Jacob E, Deutscher G, Garik P, Goldenfeld N D and Lareah Y 1986 *Phys. Rev. Lett.* **57** 1903–6
Bennemann C, Donati C, Baschnagel J and Glotzer S C 1999 *Nature* **399** 246–9
Blendell J E, Carter W C and Handwerker C A 1999 *J. Am. Ceram. Soc.* **82** 1889–900
Boettinger W J, Coriell S R, Greer A L, Karma A, Kurz W, Rappaz M and Trivedi R 2000 *Acta Mater.* **48** 43–7
Boettinger W J, Warren J A, Beckermann C and Karma A 2002 *Annu. Rev. Mater. Res.* **32** 163–94
Bragard J, Karma A, Lee Y H and Plapp M 2002 *Interface Sci.* **10** 121–6
Broughton J Q, Gilmer G H and Jackson K A 1982 *Phys. Rev. Lett.* **49** 1496–500
Caginalp G 1986 *Application of Field Theory to Statistical Mechanics* ed L Garrido (Berlin: Springer) p 216
Caginalp G and Jones J 1995 *Ann. Phys.* **237** 66–107
Cahn J W 1996 *Proc. MRS Symp. on Thermodynamics and Kinetics of Phase Transformations (Boston, MA, 1995)* vol 398 (Pittsburg, PA: Materials Research Society) pp 425–38
Cahn J W 1997 *Trans. Indian Inst. Met.* **50** 573–80
Cahn R V 2001 *The Coming of Materials Science* (Oxford: Pergamon)
Castro M 2003 *Phys. Rev.* B **67** 035412
Chang I and Sillescu H 1997 *J. Phys. Chem.* B **101** 8794–801
Chatain D, Wynblatt P, Hagege S, Siem E J and Carter W C 2001 *Interface Sci.* **9** 191–7
Chen L Q 2002 *Annu. Rev. Mater. Res.* **32** 113–40
Christian J W 1981 *The Theory of Transformations in Metals and Alloys* (Oxford: Pergamon)
Collins J B and Levine H 1985 *Phys. Rev.* B **31** 6119–22
Conti M 1997 *Phys. Rev.* E **56** 3197–202
Conti M 1998 *Phys. Rev.* E **58** 6101–8
Davidchack R L and Laird B B 1998 *J. Chem. Phys.* **108** 9452–62
Debierre J M, Karma A, Celestini F and Guerin R 2003 *Phys. Rev.* E **68** 041604
Donati C, Douglas J F, Kob W, Plimpton S J, Poole P H and Glotzer S C 1998 *Phys. Rev. Lett.* **80** 2338–41
Drolet F, Elder K R, Grant M and Kosterlitz J M 2000 *Phys. Rev.* E **61** 6705–20
Eggleston J J, McFadden G B and Voorhees P W 2001 *Physica* D **150** 91–103
Elder K R 2004 personal communication
Elder K R, Drolet F, Kosterlitz J M and Grant M 1994 *Phys. Rev. Lett.* **72** 677–80
Elder K R and Grant M 2004 *Phys. Rev.* E at press
(Elder K R and Grant M 2001 *Preprint* cond-mat/0107381)
Elder K R, Katakowski M, Haataja M and Grant M 2002 *Phys. Rev. Lett.* **88** 245701
Emmerich H 2003 *The Diffuse Interface Approach in Materials Science* (Heidelberg: Springer)
Fan D and Chen L Q 1996 *Acta Mater.* **45** 611–22
Ferreiro V, Douglas J F, Warren J A and Karim A 2002 *Phys. Rev.* E **65** 051606
Fleury V 1997 *Nature* **390** 145–8
Folch R and Plapp M 2003 *Phys. Rev.* E **68** 010602
Glicksman M E and Vold C L 1969 *Acta Metall.* **17** 1–11
Gránásy L, Börzsönyi T and Pusztai T 2002a *Phys. Rev. Lett.* **88** 206105
Gránásy L, Börzsönyi T and Pusztai T 2002b *J. Cryst. Growth* **237–239** 1813–7
Gránásy L, Börzsönyi T and Pusztai T 2003a *Interface and Transport Dynamics, Computational Modelling* (*Lecture Notes in Computational Science and Engineering* vol 32) ed H Emmerich *et al* (Berlin: Springer) pp 190–5
Gránásy L, Börzsönyi T, Pusztai T and James P F 2001 *Proc. 1st Int. Symp. on Microgravity Research and Applications in Physical Sciences and Biotechnology* vol ESA SP-454, ed B Schürmann (Noordwijk: ESA Publications Division) pp 629–36
Gránásy L and Pusztai T 2002 *J. Chem. Phys.* **117** 10121–4

Gránásy L and Pusztai T 2004 unpublished
Gránásy L, Pusztai T, Börzsönyi T, Warren J A and Douglas J F 2004 *Nature Mater.* **3** 645–50
Gránásy L, Pusztai T, Tóth G, Jurek Z, Conti M and Kvamme B 2003b *J. Chem. Phys.* **119** 10376–82
Gránásy L, Pusztai T, Warren J A, Börzsönyi T, Douglas J F and Ferreiro V 2003c *Nat. Mater.* **2** 92–6
Grier D, Ben-Jacob E, Clarke R and Sander L M 1986 *Phys. Rev. Lett.* **56** 1264–7
Gunton J D, San Miguel M and Sahni P 1983 *Phase Transitions and Critical Phenomena* vol 8, ed C Domb and J L Lebowitz (London: Academic) pp 267–466
Halsey T C 2000 *Phys. Today* **53** 36–41
Hohenberg P C and Halperin B I 1977 *Rev. Mod. Phys.* **49** 435–79
Howe J M 1996 *Phil. Mag.* A **74** 761–75
Hoyt J J and Asta M 2002 *Phys. Rev.* B **65** 214106
Hoyt J J, Asta M and Karma A 2003 *Mater. Sci. Eng. Rep.* R **41** 121–63
Huisman W J, Peters J F, Zwanenburg M J, de Vries S A, Derry T E, Abernathy D and van der Veen J F 1997 *Nature* **390** 379–81
Jou H and Lusk M T 1997 *Phys. Rev.* B **55** 8114–21
Karma A 1994 *Phys. Rev.* E **49** 2245–50
Karma A 2001 *Phys. Rev. Lett.* **87** 115701
Karma A and Rappel W-J 1996 *Phys. Rev.* E **53** R3017–20
Karma A and Rappel W-J 1998 *Phys. Rev.* E **57** 4323–49
Karma A and Rappel W-J 1999 *Phys. Rev.* E **60** 3614–25
Keith H D and Padden F J 1963 *J. Appl. Phys.* **34** 2409–21
Keith H D, Padden F J Jr and Vadimisky R G 1966 *J. Polym. Sci.* A-2 **4** 267
Keller A and Waring J R S 1955 *J. Polym. Sci.* **17** 447–72
Khachaturyan A G 1983 *Theory of Structural Transformation in Solids* (New York: Wiley)
Khachaturyan A G 1996 *Phil. Mag.* A **74** 3–14
Kobayashi R 1993 *Physica* D **63** 410–23
Kobayashi R 1994 *Exp. Math.* **3** 59–81
Kobayashi R and Giga Y 1999 *J. Stat. Phys.* **95** 1187–221
Kobayashi R and Giga Y 2001 *Japan. J. Ind. Appl. Math.* **18** 207–30
Kobayashi R, Warren J A and Carter W C 1998 *Physica* D **119** 415–23
Kobayashi R, Warren J A and Carter W C 2000 *Physica* D **140** 141–50
Krill C E and Chen L Q 2002 *Acta Mater.* **50** 3057–73
Kurz W and Fisher D J 1989 *Fundamentals of Solidification* (Lausanne: Trans. Tech.)
Laird B B and Haymet A D J 1992 *Chem. Rev.* **92** 1819–37
Langer J S 1986 *Directions in Condensed Matter Physics* ed G Grinstein and G Mazenko (Philadelphia, PA: World Scientific) p 164
Lee K and Losert W 2004 personal communication
Lereah Y, Zarudi I, Grünbaum E, Deutscher G, Buldyrev S V and Stanley H E 1994 *Phys. Rev.* E **49** 649–56
Lewis D, Pusztai T, Gránásy L, Warren J A and Boettinger W J 2004 *J. Met.* **56** 34–9
Lo T S, Dobler S, Plapp M, Karma A and Kurz W 2003 *Acta Mater.* **51** 599–611
Lo T S, Karma A and Plapp M 2001 *Phys. Rev.* E **63** 031504
Lobkovsky A E and Warren J A 2001 *Phys. Rev.* E **63** 051605
Löchte L, Gitt A, Gottstein G and Hurtado I 2000 *Acta Mater.* **48** 2969–84
Loginova I, Amberg G and Ågren J 2001 *Acta Mater.* **49** 573–81
Lotz B and Wittmann J C 1986 *J. Polymer Sci.* B **24** 1541–58
Magill J H 2001 *J. Mater. Sci.* **36** 3143–64
Masuhr A, Waniuk T A, Busch R and Johnson W L 1999 *Phys. Rev. Lett.* **82** 2290–3
Morin B, Elder K R, Sutton M and Grant M 1995 *Phys. Rev. Lett.* **75** 2156–9
Nestler B and Wheeler A A 2000 *Physica* D **138** 114–33
Ngai K L, Magill J H and Plazek D J 2000 *J. Chem. Phys.* **112** 1887–92
Nobel B D and James P F 2003 personal communication
Ode M, Kim S G and Suzuki T 2001 *ISIJ Int.* **41** 1076–82
Ojeda J R and Martin D C 1993 *Macromolecules* **26** 6557–65
Oxtoby D W 1991 *Liquids, Freezing and Glass Transition* ed J P Hansen *et al* (Amsterdam: Elsevier) pp 145–91
Oxtoby D W 2002 *Annu. Rev. Mater. Res.* **32** 39–52
Padden F J and Keith H D 1965 *J. Appl. Phys.* **36** 2987–95
Pavlik S G and Sekerka R F 1999 *Physica* A **268** 283–90
Pavlik S G and Sekerka R F 2000 *Physica* A **277** 415–31

Penrose O and Fife P C 1990 *Physica* D **43** 44–62
Plapp M and Karma A 2002 *Phys. Rev.* E **66** 061608
Pradell T, Crespo D, Clavaguera N and Clavaguera-Mora M T 1998 *J. Phys.: Condens. Matter* **10** 3833–44
Rappaz M, Jacot A and Boettinger W J 2003 *Metall. Mater. Trans.* A **34** 467–79
Roy A, Rickman J M, Gunton J D and Elder K R 1998 *Phys. Rev.* E **56** 2610–7
Rössler E 1990 *Phys. Rev. Lett.* **65** 1595–8
Ryshchenkow G and Faivre G 1988 *J. Non-Cryst. Solids* **87** 221–35
Shen Y C and Oxtoby D W 1996 *J. Chem. Phys.* **105** 6517–24
Shih W H, Wang Z Q, Zeng X C and Stroud D 1987 *Phys. Rev.* A **35** 2611–8
Simmons J P, Shen C and Wang Y 2000 *Scr. Mater.* **43** 935–42
Steinbach I, Pezzola F, Nestler B, Seesselberg M, Prieler R, Schmitz G J and Rezende J L L 1996 *Physica* D **94** 135–47
Suzuki T, Ode M, Kim S G and Kim W T 2002 *J. Cryst. Growth* **237–239** 125–31
Swallen S F, Bonvallet P A, McMahon R J and Edinger M D 2003 *Phys. Rev. Lett.* **90** 015901
ten Wolde P R, Ruiz-Montero M J and Frenkel D 1995 *Phys. Rev. Lett.* **75** 2714–7
ten Wolde P R, Ruiz-Montero M J and Frenkel D 1996 *J. Chem. Phys.* **104** 9932–47
Turnbull D 1952 *J. Chem. Phys.* **20** 411–24
Uehara T and Sekerka R F 2003 *J. Cryst. Growth* **254** 251–61
van Kampen 2003 *Stochastic Processes in Physics and Chemistry* (Amsterdam: North-Holland) pp 219–43
Vicsek T 1989 *Fractal Growth Phenomena* (Singapore: World Scientific)
Wang S L, Sekerka R F, Wheeler A A, Murray B T, Coriell S R, Braun R J and McFadden G B 1993 *Physica* D **69** 189–200
Wang Y, Jin Y M and Khachaturyan A G 2003 *Acta Mater.* **51** 4209–23
Warren J A and Boettinger W J 1995 *Acta Metall. Mater.* **43** 689–703
Warren J A, Kobayashi R, Lobkovsky A E and Carter W C 2003a *Acta Mater.* **51** 6035–58
Warren J A, Loginova I, Gránásy L, Börzsönyi T and Pusztai T 2003b *Proc. Modeling of Casting, Welding and Advanced Solidification Processes* ed D Stefanescu *et al* (Warrendale, PA: TMS Publications) pp 45–52
Wen Y H, Wang Y and Chen L Q 1999 *Acta Mater.* **47** 4375–86
Wheeler A A, McFadden G B and Boettinger W J 1996 *Proc. R. Soc.* A **452** 495–525